STRUCTURAL BEHAVIOR OF NON-PNEUMATIC TIRES USING FINITE ELEMENT ANALYSIS

by

Mesutcan Azer

B.S., Mechanical Engineering, Marmara University, 2015

Submitted to the Institute for Graduate Studies in
Science and Engineering in partial fulfillment of
the requirements for the degree of
Master of Science

Graduate Program in Computational Science and Engineering

Boğaziçi University

2023

ACKNOWLEDGEMENTS

I would like to express my sincere appreciation to my supervisor Prof. Şebnem Özüpek for her supervision, guidance, advice, criticism, support, and insight throughout this thesis and my graduate career. I am surely grateful to Assoc. Prof. Ali Ecder and Assist. Prof. Alpay Oral for being on my M.Sc. defense committee.

I owe a depth to my mom, dad, mother-in-law, father-in-law and sister for their unlimited support, unconditional love and their always smiling faces and I feel deeply grateful to my wife, love of my life Bersu Bastuğ Azer for her care, support, endless love, showing me the light even in the darkest times not only throughout my master's education but throughout whole my life.

I sincerely want to dedicate this thesis to my wife and my family for their support through the sleepless days and nights and their unconditional love.

ABSTRACT

STRUCTURAL BEHAVIOR OF NON-PNEUMATIC TIRES USING FINITE ELEMENT ANALYSIS

Modern tire technology has revolutionized vehicle performance in terms of safety and comfort by combining improvements in production techniques, materials, and design. However, conventional tires have major drawbacks like punctures, pressure loss, and temperature fluctuations, leading to a reduction in efficiency and an increase in maintenance requirements. In order to overcome these limitations, the development of non-pneumatic tire (NPT) technology has gained importance. NPTs have been characterized by their airless design using durable materials such as solid rubber or foam with major advantages like puncture resistance, minimal maintenance, and excellent load-bearing capability. This study focuses on the structural behavior of the Michelin Unique Puncture-Proof Tire System (UPTIS) based NPT using the finite element analysis. For static vertical loading, the effects of collapsible spoke thickness, spoke angle, and reinforcement thickness on the vertical displacement, vertical stiffness, contact pressure, and rolling resistance are evaluated. Additionally, the steady-state rolling analysis of NPT is performed in order to investigate the dynamic characteristics which are contact pressure and shear stress distribution on the contact area in braking, free-rolling, and traction states. As UPTIS and NPTs have been gaining more popularity in the automotive industry, the findings of this study contribute to understanding of the relationship between design parameters and NPT performance.

ÖZET

SONLU ELEMANLAR ANALİZİ İLE HAVASIZ LASTİKLERİN YAPISAL DAVRANIŞI

Modern lastik teknolojisi, üretim tekniklerindeki gelişmeler, malzemeler ve tasarımdaki iyileştirmelerin birleşmesiyle araç performansını güvenlik ve konfor açısından devrimleştirmiştir. Ancak geleneksel lastikler delinme, basınç kaybı ve sıcaklık dalgalanmaları gibi ciddi dezavantajlara sahiptir, bu da verimliliğin azalmasına ve bakım ihtiyacının artmasına neden olur. Bu sınırlamaların üstesinden gelmek için, havasız lastik teknolojisinin geliştirilmesi önem kazanmıştır. Havasız lastikler katı kauçuk veya köpük gibi dayanıklı malzemelerin kullanıldığı bir tasarıma sahiptir ve delinmeye karşı dayanıklılık, minimal bakım ve mükemmel yüke dayanma kapasitesi gibi önemli avantajlara sahiptir. Bu çalışma, Michelin Unique Puncture-Proof Tire System (UPTIS) tabanlı havasız lastiğin yapısal davranışının sonlu elemanlar analizi ile incelenmesine odaklanmaktadır. Statik dikey yük altında, katlanabilir jant kolu kalınlığı, jant kolu açısı ve güçlendirme kalınlığının, dikey rijitlik, temas basıncı ve yuvarlanma direnci üzerinde etkileri belirlenmiştir. Ayrıca, havasız lastiğin sürekli yuvarlanma durum analizi, frenleme, serbest yuvarlanma ve çekiş durumlarındaki temas basıncı ve kayma gerilimi gibi dinamik özellikleri incelemek için gerçekleştirilmiştir. UPTIS ve diğer havasız lastikler otomotiv endüstrisinde daha fazla popülerlik kazandığından, bu çalışmanın bulguları tasarım parametreleri ile havasız lastik performansı arasındaki ilişkinin anlaşılmasına katkıda bulunmaktadır.

TABLE OF CONTENTS

LIST OF FIGURES

LIST OF TABLES

LIST OF SYMBOLS

C_{10}	Temperature-dependent material coefficient
D	Distance
D_1	Temperature-dependent material parameter
F	Applied vertical force
F_R	Rolling resistance
$\bar{I}_1$	First deviatoric strain invariant
J	Total volume ratio
J^{el}	Elastic volume ratio
J^{th}	Thermal volume ratio
K	Vertical stiffness
K_0	Bulk modulus
R_e	Effective rolling radius
S	Slip ratio
U	Strain energy per unit volume
V	Ground velocity
W_d	Energy lost or dissipated
δ	Deformation
ε^{th}	Linear thermal expansion strain
$\bar{\lambda}_i$	Deviatoric stretches
μ_0	Initial shear modulus
ω	Horizontal angular velocity
Ω	Vertical angular velocity

LIST OF ACRONYMS/ABBREVIATIONS

2D	Two Dimensional
3D	Three Dimensional
FE	Finite Element
FEA	Finite Element Analysis
ME	Mechanical Elastic
NPT	Non-Pneumatic Tire
PU	Polyurethane
UPTIS	Unique Puncture-Proof Tire System

1. INTRODUCTION

1.1. Feature of NPTs

Nowadays, tires have reached a remarkable stage of development, embodying the progress made in tire technology. Due to improvements in production techniques, materials, and design, modern tires provide better performance, durability, and safety. They are specifically designed to provide excellent traction, handling, and braking on various road surfaces, ensuring a confident driving experience. Moreover, there are specialized tire versions available to provide specific needs, such as high-performance tires for sports cars, all-season tires for everyday use, and off-road tires for adventurous journeys. Also, manufacturers have integrated innovative features like run-flat capabilities, tire pressure monitoring systems, and self-sealing tires to enhance safety and convenience. Overall, the current tire landscape showcases an industry dedicated to pushing boundaries, adopting sustainability practices, and continuously improving the driving experience for drivers worldwide.

Even though there have been major technological developments in conventional tire production, the performance of air-filled tires can be impacted by punctures and leaks, which can cause a loss of pressure. Even minor changes in air pressure can result in decreased fuel efficiency and poor handling. Additionally, fluctuations in air pressure due to changes in temperature can further impact tire efficiency and performance. Regular monitoring and adjustments are necessary to maintain optimal air pressure, which raises the overall maintenance requirement and expense. The given situations make conventional tires inefficient and unreliable. Therefore, alternative tire technologies which can supply durability and performance have been explored by researchers and manufacturers.

One of the potential alternatives to pneumatic tires is a non-pneumatic tire (NPT). NPTs are made of durable materials like solid rubber or foam to provide sup-

port, stability, and grip without the need for air pressure. NPTs, also known as airless tires, are getting more popular day by day because of their advantages over conventional pneumatic tires. These can be counted as puncture resistance, low maintenance, excellent load-bearing capacity, and durability. Additionally, NPTs offer increased durability because they are made to withstand harsh environments and rocky terrain without the risk of losing air pressure. Moreover, NPTs have the potential to be more environmentally friendly by reducing tire disposal and minimizing the release of harmful microplastics. All of these make NPTs a promising alternative to pneumatic tires. NPTs are used in off-road vehicles, military vehicles, industrial equipment, bicycles, and even space vehicles. Additionally, NPT design, simulation, and optimization have been investigated for lunar or off-road environments. The researchers are interested in various aspects such as wheel design, obstacle interaction, dynamic impact simulation, rolling resistance minimization, and numerical simulation of innovative tire designs [1–5].

In order to perform at their best, NPTs' design elements cover a variety of topics that demand research. First, NPTs' load-bearing capacity, stability, and general functionality are all heavily influenced by their geometry. The shape and configuration of the tread pattern, sidewall design, and internal support structures, as well as other structural aspects of the tire, would be studied by researchers. An important factor to take into account is the material make-up of NPTs. The durability, ability to absorb shock, and resistance to wear and tear of the tire are all influenced by the material selection. Advancements in NPT technology may result from research into the properties of various materials, including solid rubber compounds, foam composites, and novel polymer blends.

It is crucial to consider various characteristics when assessing the performance of NPTs. Tire deformation, which refers to how the tire adjusts to the road surface under load, is an important factor. NPTs generally exhibit less deformation compared to pneumatic tires, enhancing stability and responsiveness. Tire stiffness, determining the ability to transmit forces, can be tailored for specific applications, balancing com-

fort, traction, and handling. Rolling resistance is another significant aspect affecting fuel efficiency and energy consumption, which can be reduced through innovative materials and tread designs. Traction, braking performance, and noise generation are also studied to ensure satisfactory performance in different road and weather conditions. Understanding these tire performance characteristics is essential for advancing NPT technology and improving overall functionality.

Durability, specifically the lifespan of NPTs, is a crucial aspect of their design and performance. Traditional tires, made of rubber filled with air, usually have a lifespan ranging from 64,000 to 128,000 kilometers. NPTs are designed to be more durable and puncture-resistant due to the lack of an air-filled chamber, potentially leading to a longer lifespan. However, currently, they are not able to reach the lifetime of pneumatic tires. Ongoing research focuses on optimizing material composition, tread design, and overall construction to extend the lifespan of NPTs.

Finite element analysis (FEA) is one of the best tools that provide the simulation of the NPTs' behavior under different loading conditions. Therefore, the effect of different design parameters on the NPT's performance can be studied via FEA.

In this thesis, FEA of a particular NPT based on the Michelin Unique Puncture-Proof Tire System (UPTIS) [6] is carried out. UPTIS was launched by Michelin and General Motors in 2019 as the first commercially available NPT for passenger automobiles. By 2024, it is anticipated that UPTIS will be extensively utilized in passenger vehicles.

The rubber-based composite structure and the tread are the two essential components of the UPTIS, as shown in Figure 1.1. The rubber-based composite structure consists of the inner hub, collapsible spoke, reinforcement ring, and outer ring. The inner hub is intended to offer a solid base and support for the whole wheel assembly. Collapsible spokes are connected to the inner hub. These spokes are made to absorb shocks and vibrations that occur during vehicle operation, improving stability

and overall comfort. The use of a collapsible design allows the spokes to retract under intense pressure, lowering the possibility of wheel damage and enhancing occupant safety. A reinforcement ring is positioned between the outer ring and tread to increase the strength and toughness of the wheel. This ring offers extra structural support and aids in evenly dispersing the load across the entire wheel, reducing the risk of any particular area of the wheel being subjected to undue stress. By strengthening the composite structure, the reinforcement ring improves the wheel's overall resilience and durability and enables it to withstand a variety of loads and road conditions. The reinforcement ring connects to the tread and outer ring of the rubber-based composite structure, ensuring effective power transmission and improving grip. It enhances the performance and aesthetics of the vehicle by supplying stability and enhancing handling. The goal of the study is to examine how design parameters affect tire performance and provide insights into the behavior of the NPT under different load conditions.

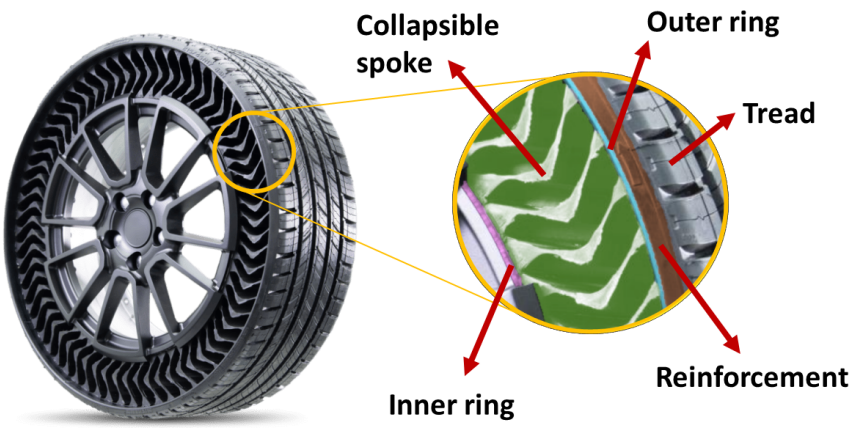

Figure 1.1. The Parts of Michelin UPTIS [6].

1.2. Literature Review

Designing an NPT is difficult and complex. The primary design factors investigated in previous research and the crucial aspects of material modeling are reviewed in the following sections. The integration of material modeling and structural design,

emphasizing their combined influence on the overall development of NPTs is also discussed.

1.2.1. Material Modeling

The effect of different material properties on the traction, durability, and overall performance of NPTs has been investigated in several studies [7, 8]. Rubber or elastomer compounds are frequently used in the construction of NPTs because of their flexibility, resilience, resistance to wear, ability to withstand a wide range of temperatures and shock absorption. Several structural reinforcements are used to give the NPT strength and stability. To improve the tire's structural integrity, stiffness, and load distribution across the tire's surface, these materials, such as fiberglass, may be embedded within the tire's spoke and rings. In the design of reinforcements of some NPTs, metal elements like steel or aluminum are also used. Components like rims, hubs, and outer covers are frequently made of plastic, fiberglass, and carbon fiber because they are lightweight, corrosion-resistant, and simple to manufacture. For the necessary support and cushioning in some NPT designs, solid fill materials like polyurethane (PU) or foam are utilized in spokes, reinforcement ring, and outer ring. PU is a polymeric material that experiences low energy loss when it is deformed. This results in the ability to return to its original shape [9–11]. The tires are suitable for rocky terrains and heavy-duty applications thanks to these materials' excellent shock absorption capabilities.

Upon providing an introduction to the materials employed in NPTs, the subsequent emphasis is directed toward their mathematical modeling.

Rugsaj and Suvanjumrat [12] studied hyperelastic material models to present PU. The tensile and compressive uniaxial experimental results were used to calibrate the hyperelastic material model parameters. FEA of the test specimens was carried out. The predictions were in good agreement with the experiments, with averaged errors for the compressive test, using the Ogden model, and the tensile test, using the Mooney-

Rivlin model, as 17.07% and 5.61%, respectively. Since the data were used for both calibration and validation the quantitative results are not very meaningful, however, show the challenges concerning material behavior representation.

Additionally, Rugsaj and Suvanjumrat [13] created a dynamic finite element (FE) model of a rolling NPT. The PU used for the shear band and spoke was represented with a linear elastic material model combined with the generalized Maxwell's viscoelastic material model. Tensile and compressive test results on NPT specimens were used to calibrate this material model. The FE model of NPT rolling at 11 km/h on curved and flat surfaces under 14000 N vertical load was constructed. The predictions were compared to those of the actual experiment of NPT rolling on the drum testing machine under the same conditions. The comparison resulted in an average difference of 3.68% and 3.89% for rolling on curved and flat surfaces, respectively. The maximum dynamic values of the impact force at the interface between the tread and flat surface, displacement of the center of NPT, and maximum stress, which occurred at the upper part of the spoke because of tension while rolling were, respectively, 1.06, 1.16, and 1.805 times higher than the static values. The performance limitation of rolling NPT on a flat plate was then examined. For the maximum load of 20000 N and a speed of 15 km/h, the shear stress between the shear band and the spoke was predicted as 1.7277 MPa.

Kim et al. [14] also used PU as a spoke and shear band. Moreover, they selected synthetic rubber for the tread. These materials were modeled with Ogden hyperelastic material model. In their design, the hub was made of Al 7075-T6 aluminum alloy with high strength steel rings. They investigated the load-carrying capability, contact pressure, and local stress in the spoke. They observed a decrease in vertical stiffness and 30% reduced contact pressure with the hexagonal honeycomb spoke design. Similarly, Veeramurthy et al. [15] used aluminum alloy and high strength steel for inner and outer reinforcement, respectively. Moreover, both the spokes and shear beam were composed of PU with nonlinear hyperelastic material model. Additionally, Ogden strain energy potential was used for defining the hyperelastic property of synthetic rubber as the

tread's material. The model was defined using the experimental data from uniaxial, biaxial and planar tests. They optimized the design parameters such as spoke thickness and shear band thickness to minimize the rolling resistance of the NPT.

Narasimhan [16] investigated the effect of material properties of a NPT on static load deflection and vibration. He used hyperelastic Marlow material for PU ring and the spokes which was calibrated from uniaxial test data. In order to examine the effects of changing material stiffness, Mooney Rivlin and Neo Hookean material models were also studied. The sensitivity of the results to shear and bulk moduli were investigated. It was observed that in static loading decreasing the shear modulus of the ring and spokes resulted in increased vertical displacement, hence decreased stiffness, signifying a higher deformability of the NPT under the same load conditions. Comparatively, the Neo Hookean model significantly reduced the tire's stiffness, while the Mooney Rivlin model caused only a slight decrease.

1.2.2. Structural Design of NPTs

Researchers have explored the use of different structural designs to raise NPTs' performance. The honeycomb and lattice type spoke geometry has been widely investigated in the literature.

Ju et al. [17] investigated hexagonal honeycomb spokes as a design approach to enhance fatigue resistance. The focus was on identifying compliant hexagonal structures that exhibit low local stresses when subjected to macroscopic uniaxial loading. Two cases of hexagonal honeycombs were designed, one with the same cell wall thickness and the other with the same load-carrying capacity. The elastic limits of these honeycombs were determined using the ABAQUS FE code, considering geometric nonlinearity associated with cell wall buckling and bending. The investigation of local stresses under identical 20 mm vertical displacement at the center of the tires reveals that hexagonal honeycombs with a highly positive cell angle exhibit both low local stresses and low mass while maintaining the same vertical load-carrying capability.

Kucewicz et al. [18] studied a modeling methodology and FE model simulation for selected NPTs and proposed a new concept of an airless tire, KucWheel. To describe the mechanical properties of tire components, Mooney-Rivlin, which is a widely used nonlinear hyperplastic material model, was employed. A static radial deflection test was conducted under 10000 N vertical force, investigating the influence of internal structure geometry on rim vertical displacement, deformation shape, and contact pressure. The results obtained from all tested tires were compared. The Honeycomb cellular tire exhibited the smallest vertical displacement with a measurement of 21 mm, indicating the highest radial stiffness coefficient among the tested tires. Similar results were observed for the KucWheel concept, which recorded a vertical displacement of 21.6 mm. On the other hand, larger deflection values were observed for the Tweel and airless tire concepts, measuring 33.2 mm and 89 mm, respectively. Numerical investigations demonstrated that each tire exhibited distinct radial load transfer and stress distribution due to variations in their internal structure geometry, despite having the same mass across all designs. The simulations were carried out using the explicit LS-Dyna commercial code.

Mathew et al. [19] investigated a model of an airless tire, utilizing natural rubber instead of synthetic rubber in the tread and polyester instead of nylon in the carcass. The research involved a comprehensive examination of different types of airless tires, comparing them with pneumatic tires. Airless tire spokes of various structures such as honeycomb, spokes, triangular, and diamond with an applied load of 1200 N were analyzed using ANSYS software. A comparative analysis was conducted among these structures using different materials. The results revealed that the tire with a diamond structure and synthetic materials experiences less deformation in comparison to other structures. In addition, the NPTs had lots of structural differences.

Zhang et al. [20] discussed different types of NPT technology including PU, tread with plate spokes, tread with non-plate spokes, and net tread. PU tires utilized high elastic polymer-PU for load-bearing and safety. Tread with plate spokes relied on plate spokes to support the load, while the tread with non-plate spokes used specialized spoke

structures for air replacement. Net tread tires had an open tread structure and found applications in space exploration.

Kim et al. [14] studied static contact behaviors of NPTs with hexagonal honeycombs. The relationship between vertical loading and contact pressures was examined and compared with that of a pneumatic tire Three different NPTs were designed. Sequentially increasing vertical loads of 1000 N, 2000 N, 3000 N, and 4000 N were applied to the center of the tires. The NPTs' vertical force-deflection curves demonstrated that the vertical stiffness decreased with load, which was related to the cells' initially high resistance to compression and their subsequent ease in buckling. As the vertical load increased, the NPTs with the hexagonal cellular spokes exhibited lower contact pressure than pneumatic tires; in this study, a reduction of about 30% was noted at a vertical load of 3000 N due to the decreasing vertical stiffness with load.

Ju et al. [21] investigated the structural behavior of a wheel using FEA. In this study, the contact pressures of metallic cellular shear bands were examined to determine whether metallic cellular materials could replace elastomers. Different cellular geometries were analyzed under a vertical force of 625 N applied at the hub's center, was applied. Even though the aluminum alloy cellular shear bands were intended to have the same shear modulus of 6.5 MPa, different cellular geometries resulted in different nonlinear stress-strain behaviors under the large shear deformation, hence different contact pressure profiles, Additionally, with in-plane shear flexible structures, a cellular shear band designed with a higher negative cell angle results in a lower contact pressure along the contact patch.

Veeramurthy et al. [15] carried out a study related to the optimization of a NPT for reduced rolling resistance. The effects of the spoke thickness and the shear band thickness of the NPT on vertical stiffness and rolling resistance response were investigated using a FE model. For the simulation, first, a static vertical load is applied Then, a quasistatic rolling analysis was carried out to examine the time-dependent viscoelastic material response in the spoke, shear beam, and tread of the NPT. It was

found that the shear band thickness has a greater impact on the rolling resistance. Comparing the optimized result to a reference design used in earlier studies it was concluded that increasing the shear band thickness by 40% and the spoke thickness by 25%. Energy loss was reduced by 17.49%.

Zhao et al. [22] proposed a new NPT called the mechanical elastic wheel (ME-wheel). The Mooney Rivlin model was used to characterize the rubber's hyperelasticity and incompressibility, while the rebar layer was used to simulate the multilayer rubber-cord composites for the reinforcement and base. Static stiffness characteristics of the wheel with different hinge structures were investigated. Axial loads of 9500, 16500, 18500, and 21000 N were applied to examine the longitudinal, lateral, and torsional stiffnesses. It was found that the vertical stiffness of the NPT increased as the number of hinge units increased. With an increase in axial load, the longitudinal and lateral stiffness both increased. The NPT assembled with a two-link hinge has higher longitudinal stiffness than that of a three-link hinge when the number of hinge units was the same. The impact of these two various hinge designs, however, on the lateral stiffness was essentially nonexistent.

A tire's grounding characteristic is a crucial factor in ensuring the stability and safety of a vehicle. Du et al. [23] investigated the grounding characteristics of a non-pneumatic ME wheel under rolling movement with a camber angle. They conducted the stiffness tests to verify the precision of the simulation model of the ME wheel. An inflatable tire was chosen as the reference tire. The grounding properties of the ME wheel and inflatable tire were studied during free-rolling, braking, and driving conditions at a translational velocity of 10 km/h, 8000 N vertical load, and 2°, 4°, 6°, and 12° camber angles. According to their FEA and experimental research, as the camber angle increased, both tires (ME wheel and inflatable tire) experienced tread surface wear. However, the inflatable tire suffered more severely from the pressure concentration. This study is beneficial for enhancing the design and evaluation of the mechanical performance of the ME wheel.

The study of the tire's lateral mechanics is essential as it determines the tire's stability during lateral maneuvers, such as cornering or lane changing, therefore, impacting the overall safety of a vehicle. Hongxun et al. [24, 25] conducted a theoretical and numerical analysis of the ME wheel to optimize the lateral stiffness. In the study, 10000 N,15000 N, and 20000 N vertical loads were used. They exhibited that increasing the vertical load enhanced the cornering stiffness, lateral force, and torque of wheel. Additionally, they demonstrated that by increasing the depth-to-width ratio of the tire bead section, the lateral stiffness of the ME wheel decreased. Additionally, Pewekar and Gaikwad [26] explored the deformation mechanisms of NPTs under four cases of loading which were uniaxial compressive, lateral shear, lateral torsion, and circumferential torsion. They quantified the strength of pneumatic tire and NPT under those load conditions. They observed that NPT had outstanding torsional stiffness, however, it suffered from lateral stiffness. Therefore, more research should be concentrated to improve the lateral stiffness of NPT.

Similarly, Zhao et al. [27] carried out a study related to the natural dynamic characteristics and influencing factors of a non-pneumatic ME wheel for an off-road vehicle. The FE model of the wheel was constructed and the model's validity was confirmed by a load characteristic test. For this test, 2000 N, 4000 N, 6000 N, 8000 N, 10000 N, and 12000 N were used as vertical loads. Analysis was done on how mode shapes and natural frequencies were affected by ground constraints, material properties, vertical load, and driving torque. It was found that the natural frequency of the wheel increased with an increase in the elastic modulus of elastic rings, loads, and torques; and ground constraints clearly affected the intensity of the vibration.

Additionally, using Taguchi's parameter design method [28] and orthogonal arrays, it was found that several important spoke and ring geometric parameters had a significant impact on vibration [29, 30]. To simulate the rolling of the NPT, a two-dimensional (2D) planar FE model with geometric nonlinearity and explicit time-stepping was used. The frequency spectrum of the time signals of the perpendicular distance of the marker nodes from the virtual plane of the spoke, ground reaction forces,

and ring vibration were used to determine the vibration characteristics. The findings demonstrated that Tweel vibration was significantly reduced by both shortening the spokes and bending them more radially.

1.3. The Objective of the Study

The goal of this thesis is to investigate the effect of the selected design factors on the performance of an NPT based on the Michelin UPTIS.

In particular, three design parameters are considered: spoke thickness, spoke angle, and reinforcement thickness. The effect of the selected parameters on the response are evaluated for the following quantities: Vertical deformation, vertical stiffness, contact pressure, and rolling resistance. Static analysis is performed for vertical loading that represents the weight of the vehicle. In addition, steady-state analysis is carried out for free-rolling, traction, and braking.

Vertical deformation is crucial in determining the system's structural stability and deformation characteristics. The ability to withstand external forces, rigidity, and susceptibility to deformation or failure of the system can all be evaluated by analyzing the impact of particular parameters on vertical deformation. The vertical stiffness of a system is a measure of its resistance to vertical deformation or compression. It determines the NPT's ability to support loads and maintain its shape in the face of vertical forces. Contact pressure shows how forces are distributed between interacting surfaces. High contact pressures can cause materials to wear out, to deform locally, or even to become damaged. The design and material properties can be optimized to reduce excessive contact pressures. Rolling resistance is an important parameter in many applications, especially in the automotive and transportation sectors. More energy is needed to overcome higher rolling resistance, which in turn increases fuel consumption, decreases efficiency, and increases wear and tear. It is possible to determine how to reduce rolling resistance by optimizing tire design, using materials with lower rolling resistance, or changing operating conditions by analyzing the impact of a few selected

parameters on rolling resistance.

The results of the study contribute to the development of more dependable and effective NPTs that have the potential to revolutionize the tire industry and raise vehicle efficiency and safety. Moreover, the study offers a framework for NPT research in the future promoting further investigation and advancement of this promising technology.

2. 3D FINITE ELEMENT NPT MODEL

A three-dimensional (3D) FE model of an NPT is presented in this chapter. The NPT is subject to static vertical loading and rolling. To observe how the NPT responds to these conditions, its vertical displacement, vertical stiffness, contact pressure, and rolling resistance are evaluated in the study. Additionally, the effects of different geometric parameters on the response are evaluated with respect to the reference NPT model. The static footprint loading and rolling analysis are performed in ABAQUS [31].

2.1. Geometry

The geometry is based on Michelin UPTIS [6]. This NPT is of size 215/45R17 and was designed for the Chevrolet Bolt EV vehicle. The designation of '215/45R17' specifically denotes a tire with a width of 215 mm, an aspect ratio of 45 for sidewall height, and a rim diameter of 17 inches. Sidewall height is calculated by taking 45% of 215 mm.

Additionally, 17 inches is equal to 431.80 mm for the inner diameter. Therefore, the tire type '215/45R17' corresponds directly to the dimensions outlined in Table 2.1. The geometry of the NPT is shown in Figure 2.1 and was created by the author in Solidworks [32], using the information that is provided on the official source of the manufacturer [6].

The NPT is made up of five components. These are tread, reinforcement (shear beam), outer ring, collapsible spoke, and inner ring (hub) as demonstrated in Figure 2.2. The tread is designed for contact between the NPT and the road. The reinforcement (shear beam) is located between the outer ring and the tread of NPT. Its main purpose is to strengthen the NPT's structural integrity.

Figure 2.1. The UPTIS NPT model constructed in Solidworks.

The outer ring, which supports the tire structure, is a part that is positioned between the reinforcement and the collapsible spoke. It serves as a firm boundary and aids in keeping the shape of the tire. When the NPT is subjected to different loads, the outer ring helps to prevent excessive deformation of the tire. The collapsible spoke located between the outer ring and the inner ring gives the NPT a unique shape and design. When the NPT comes into contact with obstructions, the collapsible spoke allows the NPT to collapse in specific places. By giving the tire flexibility and adaptability, this feature enhances shock absorption and creates a smoother ride. The geometric parameters of UPTIS tire used in this study are provided in Table 2.1.

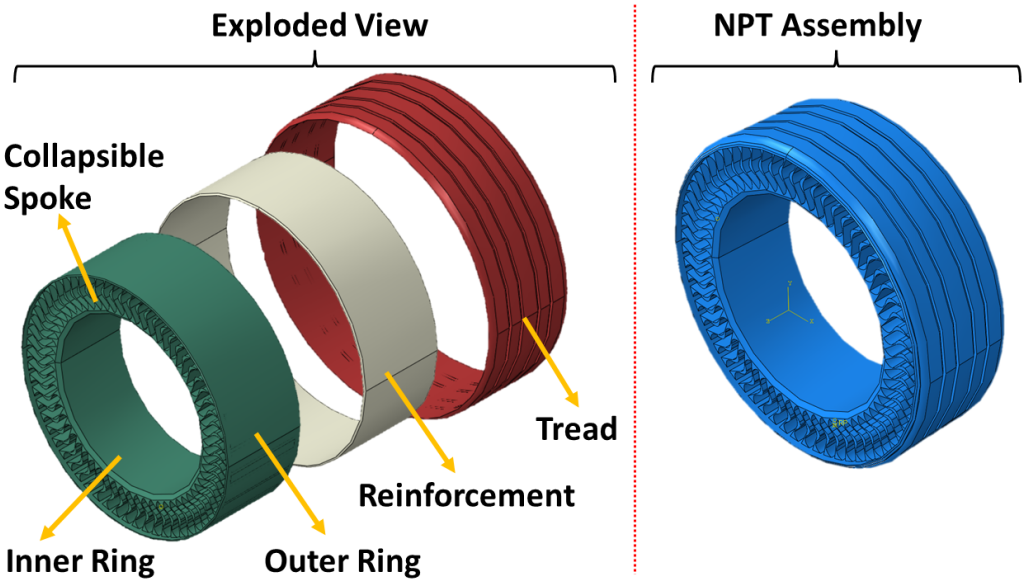

Figure 2.2. The NPT model imported to ABAQUS.

Table 2.1. The parameters of 3D NPT [6].

Parameters	**NPT Model**
Outer Diameter	625.30 mm
Inner Diameter	431.80 mm
Tread Thickness	8 mm
Reinforcement Thickness	4 mm
Outer Ring Thickness	3 mm
Inner Ring Thickness	10 mm
Spoke Inner Radius	20.5 mm
Spoke Outer Radius	9.40 mm
NPT Width	215 mm
Spoke Flat Thickness	2 mm

2.2. Material Properties

The material data for UPTIS are not available in the literature, therefore the material parameters of another type of NPT, Tweel manufactured by Michelin [33] are

used. In particular, the material models given in [16] are used.

The inner ring, collapsible spoke, and outer ring are made of PU. The tread consists of rubber material. Additionally, orthotropic reinforcement is used.

The material model that is used for the tread, outer ring, collapsible spoke, and inner ring of the NPT is an isotropic hyperelastic material model while the reinforcement is represented with an orthotropic elastic material model. Hyperelastic materials are nonlinear and isotropic. They exhibit instantaneous elastic responses up to high strain values. Elastic materials, on the other hand, can be isotropic or orthotropic and are only effective for very small elastic strains.

2.2.1. Isotropic Hyperelastic Material

The isotropic hyperelastic material model with Neo-Hookean strain energy potentials is used for the tread, rings, and collapsible spoke of the NPT. The Neo-Hookean strain energy potential form [34] is

$$U = C_{10}\left(\bar{I}_1 - 3\right) + \frac{1}{D_1}\left(J^{el} - 1\right)^2, \tag{2.1}$$

where U is the strain energy per unit volume; C_{10} and D_1 are temperature-dependent material parameters; $\bar{I}_1$ is the first deviatoric strain invariant defined as

$$\bar{I}_1 = \bar{\lambda}_1^2 + \bar{\lambda}_2^2 + \bar{\lambda}_3^2, \tag{2.2}$$

where $\bar{\lambda}_i = J^{-\frac{1}{3}}\lambda_i$ are the deviatoric stretches; J is total volume ratio; J^{el} is elastic volume ratio given by

$$J^{el} = \frac{J}{J^{th}}, \tag{2.3}$$

where J indicates the total volume ratio, and J^{th} is thermal volume ratio. The thermal volume ratio is provided by

$$J^{th} = \left(1 + \varepsilon^{th}\right)^3, \tag{2.4}$$

where ε^{th} indicates linear thermal expansion strain. The initial shear modulus (μ_0) and bulk modulus (K_0) are obtained by

$$\mu_0 = 2C_{10}, \tag{2.5}$$

$$K_0 = \frac{2}{D_1}. \tag{2.6}$$

The coefficients and initial shear modulus and bulk modulus for the tread, outer ring, collapsible spoke, and inner ring of the NPT are given in Table 2.2.

Table 2.2. Isotropic Hyperelastic Moduli for the tread, outer ring, collapsible spoke, inner ring of the NPT [16].

Component	C_{10} [**N/mm^2**]	D_1 [**mm^2/N**]	**Initial Shear Modulus [N/mm^2]**	**Initial Bulk Modulus [N/mm^2]**
Tread	0.833	0.124	1.666	16.100
Outer Ring	4.912	0.021	9.825	94.984
Collapsible Spoke	4.912	0.021	9.825	94.984
Inner Ring	4.912	0.021	9.825	94.984

2.2.2. Orthotropic Elastic Material

The material model which is used for the reinforcement is an orthotropic elastic material. Three perpendicular mirror planes in orthotropic materials produce orthotropic symmetry. Models indicate that these reinforcements are comparatively inextensible. An orthotropic material has a different Poisson's ratio in each direction. For the orthotropic material on the reinforcement, the radial direction is represented by 1111, the tangential direction is represented by 2222, and the out-of-plane direction is represented by 3333. The material coefficients are given in Table 2.3 where D indicates the material stiffness parameters.

Table 2.3. Orthotropic Elastic Moduli for reinforcements [N/mm^2] [16].

D1111	**D1122**	**D2222**	**D1133**	**D2233**	**D3333**	**D1212**	**D1313**	**D2323**
0.1	0	100	0	0	0.1	100	20	20

2.3. Mesh Properties

The tread, reinforcement, outer ring, collapsible spoke and inner ring of the NPT are modeled with linear tetrahedron element (C3D4H). Additionally, the hybrid formulation is used as PU is considered nearly incompressible. 18659 elements are used to construct the FE model of the tread as shown in Figure 2.3. The FE mesh of the reinforcement has 5263 elements as illustrated in Figure 2.4. 32916 elements are used for meshing the outer ring, collapsible spoke and inner ring together as demonstrated in Figure 2.5. Figure 2.6 shows the 3D mesh of the NPT where total of 56838 elements are created.

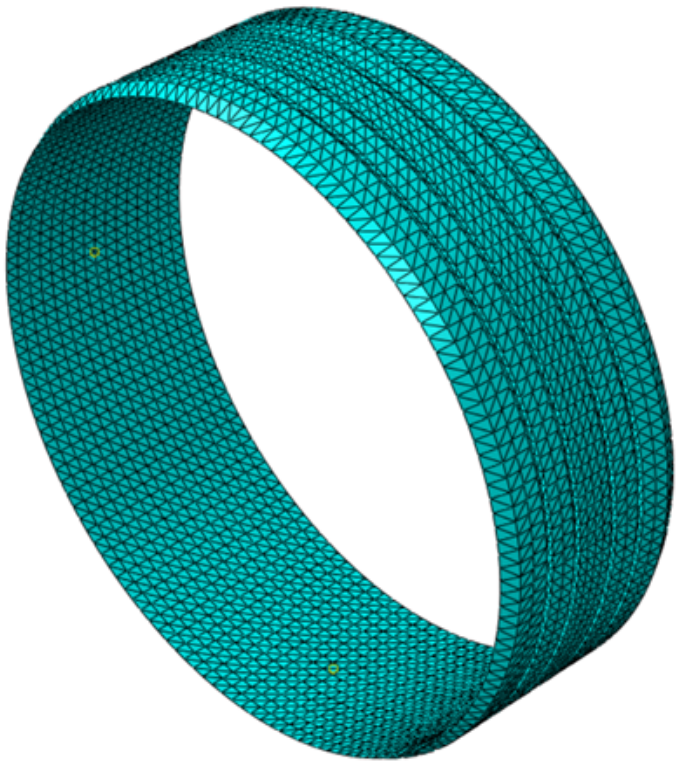

Figure 2.3. FE mesh of the tread.

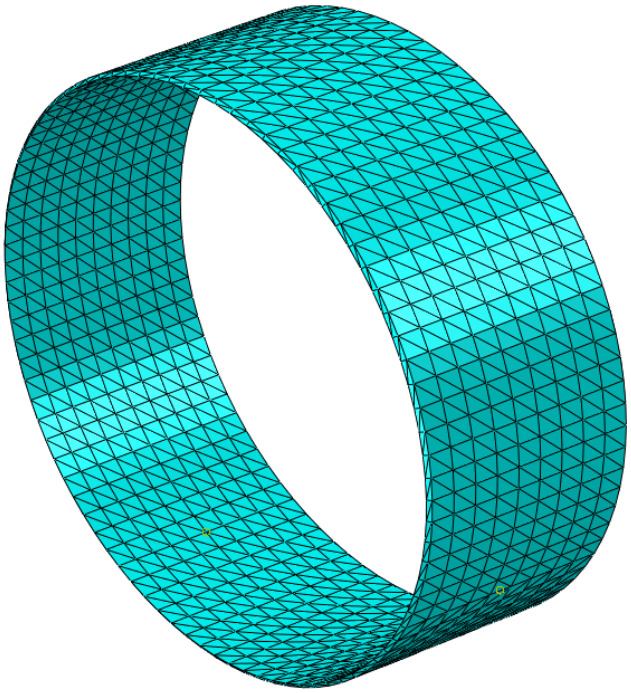

Figure 2.4. FE mesh of the reinforcement.

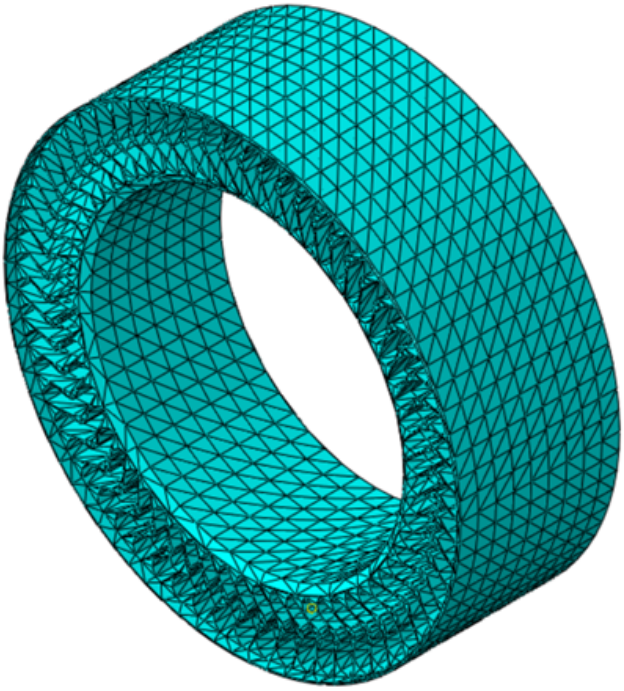

Figure 2.5. FE mesh of the outer ring, collapsible spoke, and inner ring.

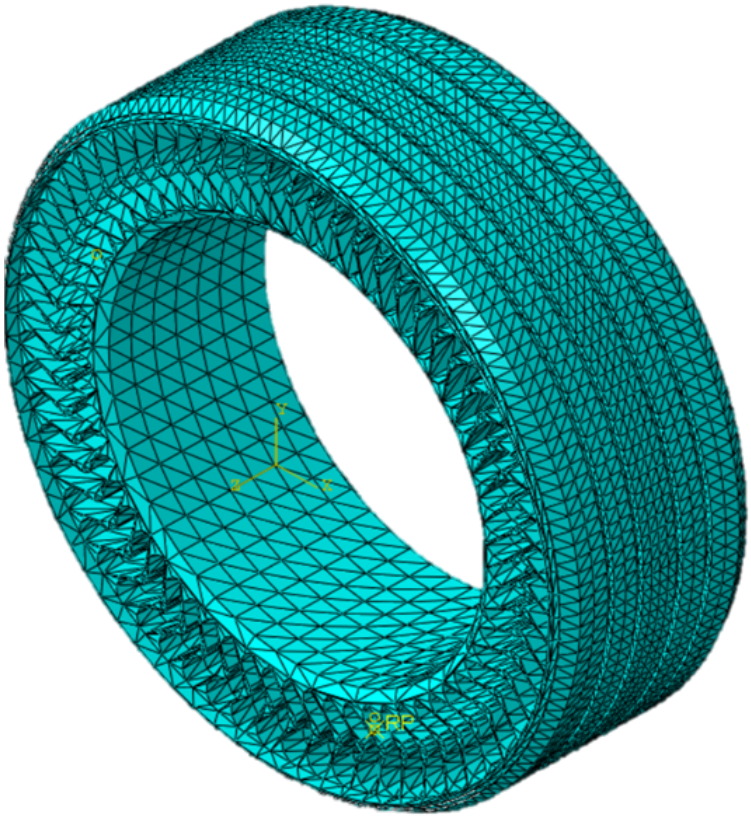

Figure 2.6. FE mesh of the NPT.

2.4. Interactions and Constraints

Interactions and constraints in the FEA of the NPT have an important role to construct the proper test model in ABAQUS.

The contact between the rigid road and the tread of NPT is assigned for the initial step. The upper surface of the road is selected as the master surface and the surface of the tread closest to the road is picked as the slave surface as demonstrated in Figure 2.7. Surface-to-surface is chosen for the discretization method. Additionally, the sliding formulation is determined as finite sliding. Normal contact behavior is defined as hard contact that is no penetration is permitted between the contacting surfaces. For static analysis, tangential behavior is selected as frictionless. For rolling analysis, shown in Figure 2.8, the coefficient of friction with value 1 is used. In addition to this, contact separation is allowed in the analysis.

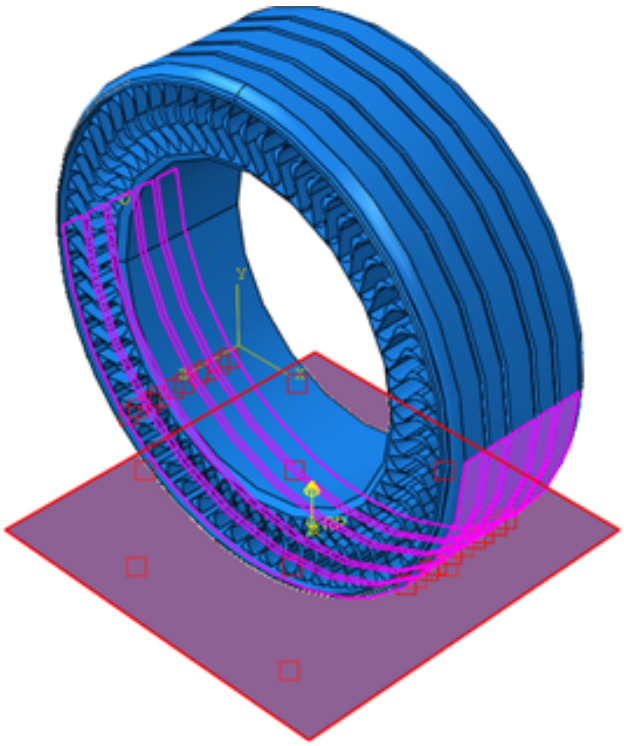

Figure 2.7. The interaction between the tread and the road surfaces in the static loading.

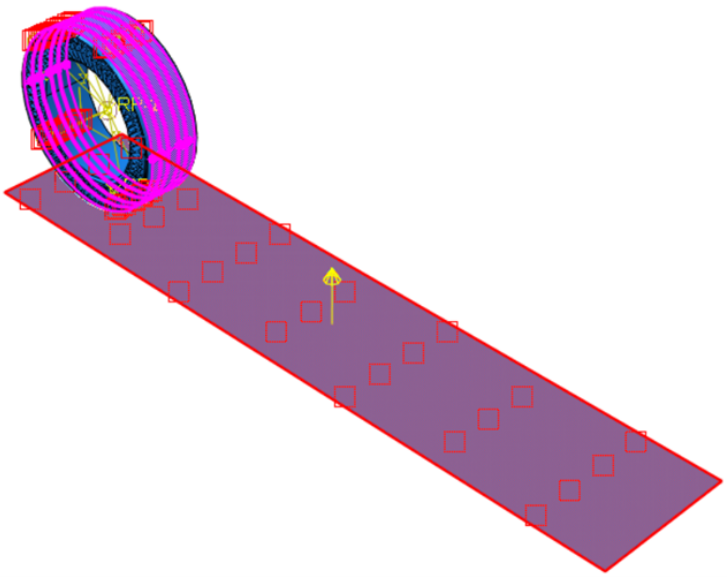

Figure 2.8. The interaction between the tread and the road surfaces in rolling analysis.

The tread and the reinforcement of the NPT are connected to each other using surface-based tie constraint as shown in Figure 2.9. The inner surface of the tread is defined as the master surface, and the bottom surface of the reinforcement is named the slave surface. The position tolerance between the tread and the reinforcement of the NPT is 0.1 mm.

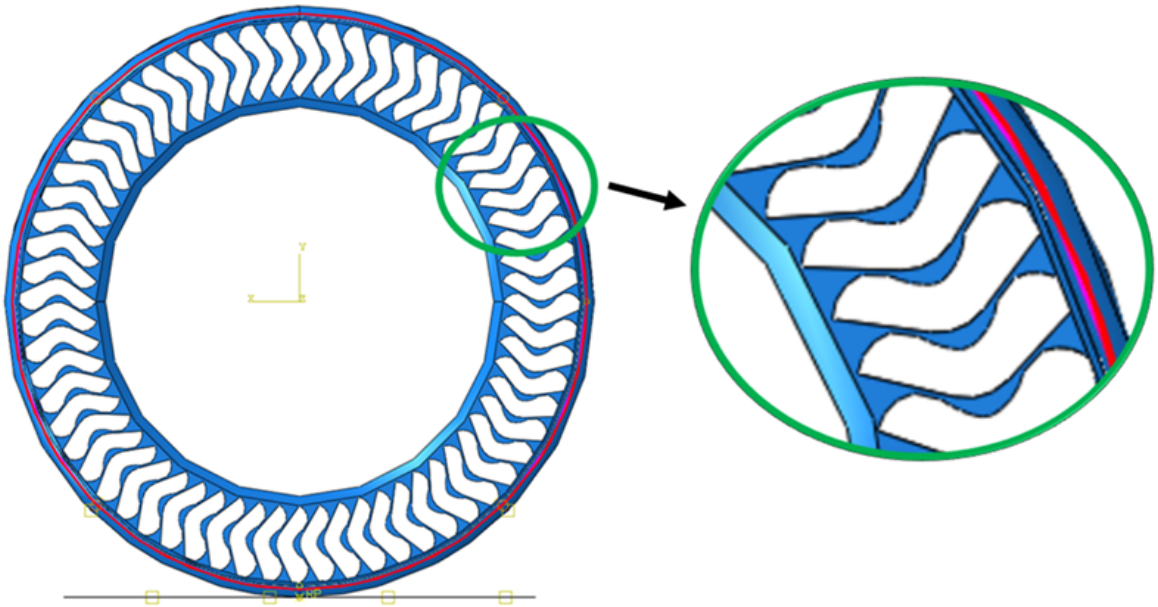

Figure 2.9. The constraint, indicated by red line, between the tread and the reinforcement surfaces.

Surface-based tie constraint is assigned to merge the reinforcement and the outer ring of the NPT as illustrated in Figure 2.10. The inside surface of the reinforcement is defined as the master surface, and the bottom surface of the outer ring is named the slave surface. For this connection, 0.1 mm position tolerance is determined. Also, the outer ring, collapsible spoke, and inner ring are already connected to each other as one model.

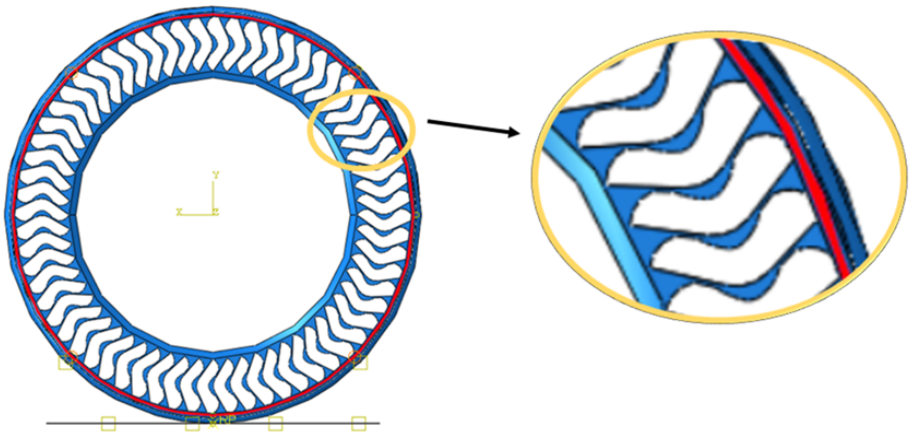

Figure 2.10. The constraint, indicated by red line, between the reinforcement and outer ring surfaces.

The interaction between the center of the NPT and the inner surface of the inner ring of the NPT is defined by kinematic coupling in ABAQUS as illustrated in Figure 2.11. To define the coupling, a reference point is established in the NPT's center.

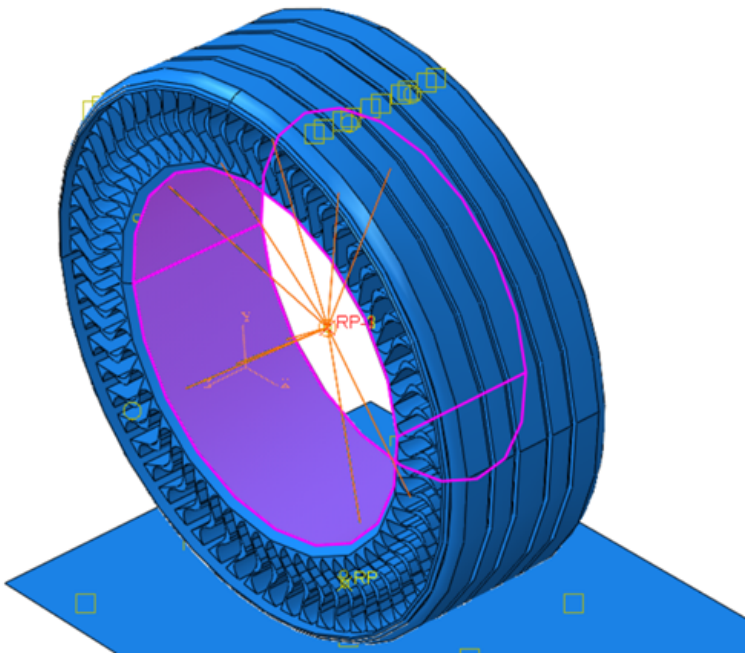

Figure 2.11. The kinematic coupling between the inner surface of the inner ring and center of the NPT.

2.5. Loads and Boundary Conditions

The vertical load to be applied is calculated from Chevrolet Bolt EV's total weight since UPTIS is developed for this specific vehicle. The base curb mass of the vehicle is 1628 kg [35]. Therefore, the load to be applied in the vertical direction for one tire is calculated as 3991.306 N. This value is taken as the minimum load to be applied on the NPT in the static loading. Two additional loads are considered as 4903.324 N and 5638.822 N. These loads correspond to 500 kg, the maximum mass UPTIS can carry [6], and 575 kg, 15% greater than the maximum mass, respectively. Only the 3991.306 N vertical load is used in the rolling tests.

The concentrated loads are applied at the surface of the road toward the NPT as shown in Figure 2.12. The center hub of the NPT is constrained in all axis and degrees for the FEA as illustrated in Figure 2.13.

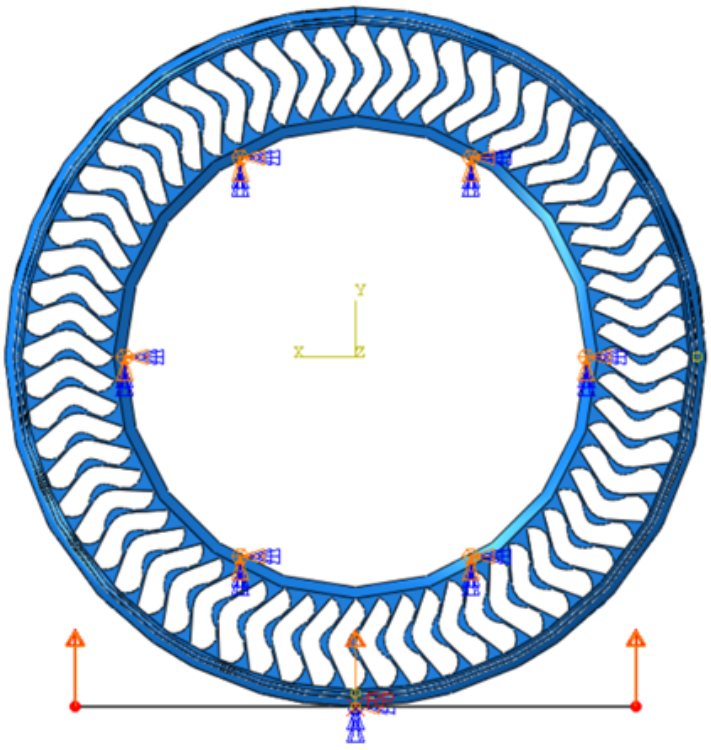

Figure 2.12. The load applied on the surface of the road.

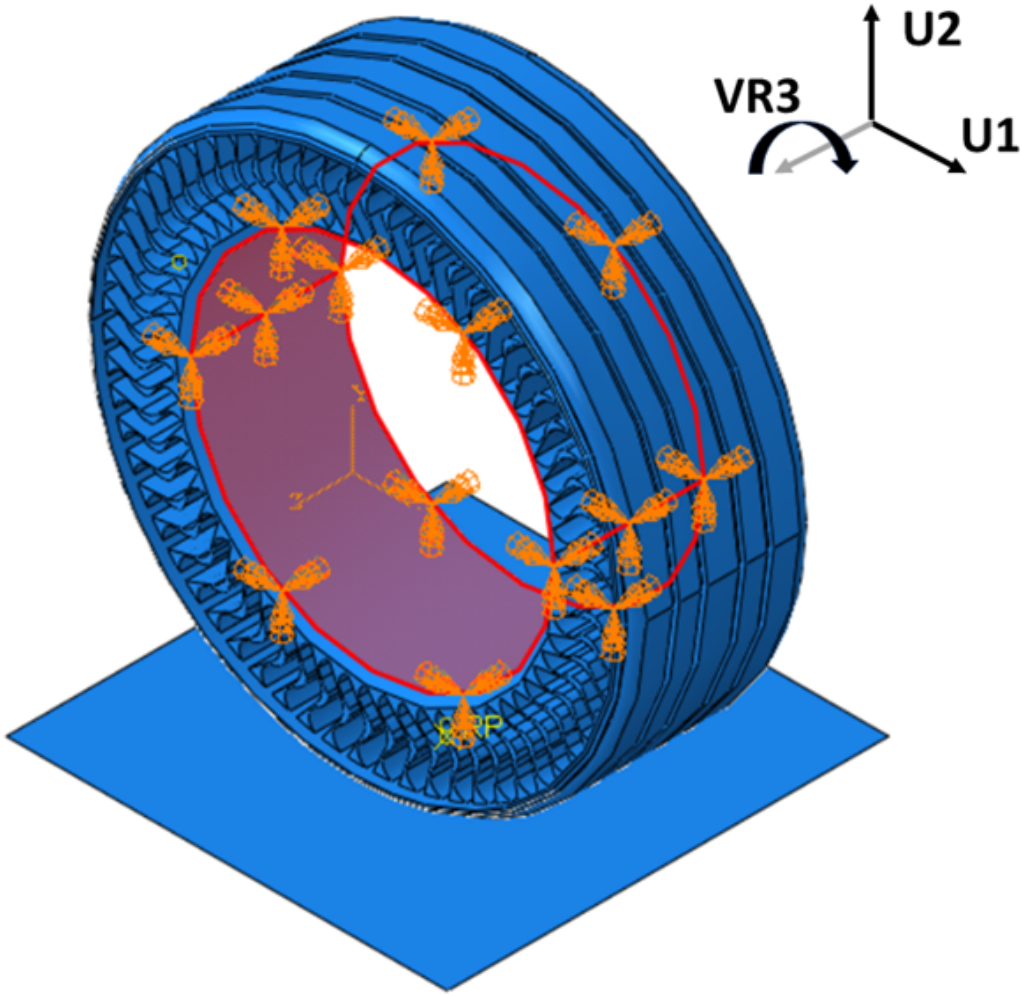

Figure 2.13. The boundary condition on the inner ring.

The rigid road is set free in the U2 direction and constrained in the other directions. In the rolling analysis, first, the vertical load is applied as a ramp load for 1 second, then, 15.984 rad/s angular velocity is prescribed as a ramp at the reference point located at the center of the tire geometry for 0.2 seconds in the negative VR3 direction as shown in Figure 2.14. This value is calculated for the NPT traveling at a speed of 18 km/h, where inertia is assumed to be negligible. During the rolling motion, the NPT is allowed to move in the U1 and VR3 directions and the total rotating distance run by the NPT is set as 1 meter.

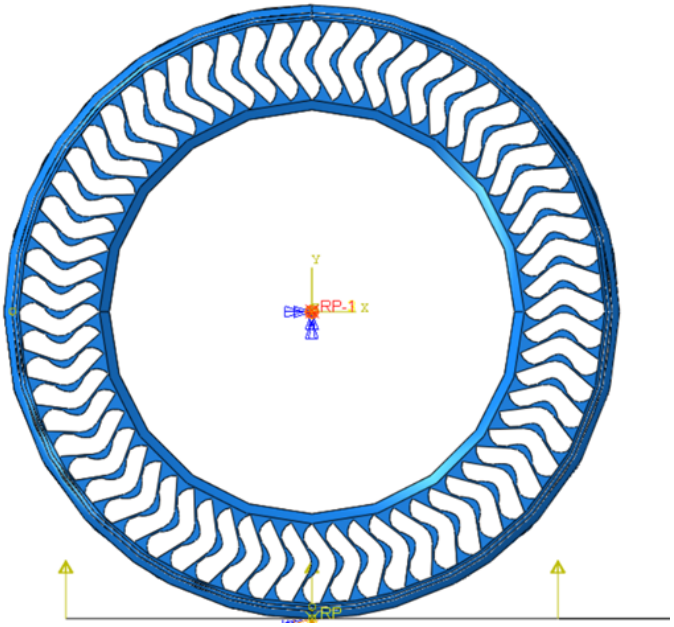

Figure 2.14. The angular velocity is applied at the reference point located at the center of the NPT.

2.6. The Evaluation of the NPT Model

In this section, to verify the accuracy of the NPT model, the vertical displacement value obtained from the static loading is compared with the reference study [16] in the literature.

Since UPTIS is still being developed by Michelin, experimental data on the tire is not available in the open literature. Therefore, a study that considers another Michelin tire is selected as a reference for comparison. The NPT used in the reference study, Tweel, is a prototype developed by Michelin for passenger vehicles [33]. Tweel and UPTIS geometries are compared in Table 2.4.

The Tweel model has the tread, ring, collapsible spoke, and inner hub. The ring is a composite structure consisting of a PU shear band sandwiched between reinforcement rings [16]. The main difference between the Tweel model used in the reference study and UPTIS model used in this study is that Tweel model has two thin orthotropic

reinforcements, while UPTIS consists of one thick orthotropic reinforcement structure. The material properties of the NPT considered in this study are taken from the reference study as detailed in Section 2.2. In other words, the material models of the two analyses are the same as detailed in Sections 2.1 and 2.2.

The same load and temperature conditions used in Tweel analysis were applied to the UPTIS-based NPT model. In the reference study, Tweel was subjected to a static footprint loading of 3665 N.

Table 2.4. Comparison of the dimensions of UPTIS and Tweel.

Parameters	**Present UPTIS Model**	**Reference Tweel Model**
Outer Diameter	625.30 mm	584 mm
Inner Diameter	431.80 mm	422 mm
Width	215 mm	210 mm

In addition to this, a predefined field is set to give the temperature value to the NPT like the reference study. Thermal expansion coefficients of ring, spoke, reinforcement and tread are 0.0002/°C, 0.0002/°C, 0.000012/°C, and 0.00017/°C, respectively. First, the temperature is set to 125 °C for the initial step. Then, the temperature is reduced to 75 °C and maintained during the load test step.

The load-displacement curves for Tweel and UPTIS models are given in Figure 2.15. Based on the comparison of the two responses the current study is verified. In addition, the close agreement of the maximum vertical displacements of Tweel and UPTIS, 11.78 mm and 11.73 mm, respectively, shows that the material model is the determining factor in the footprint analysis.

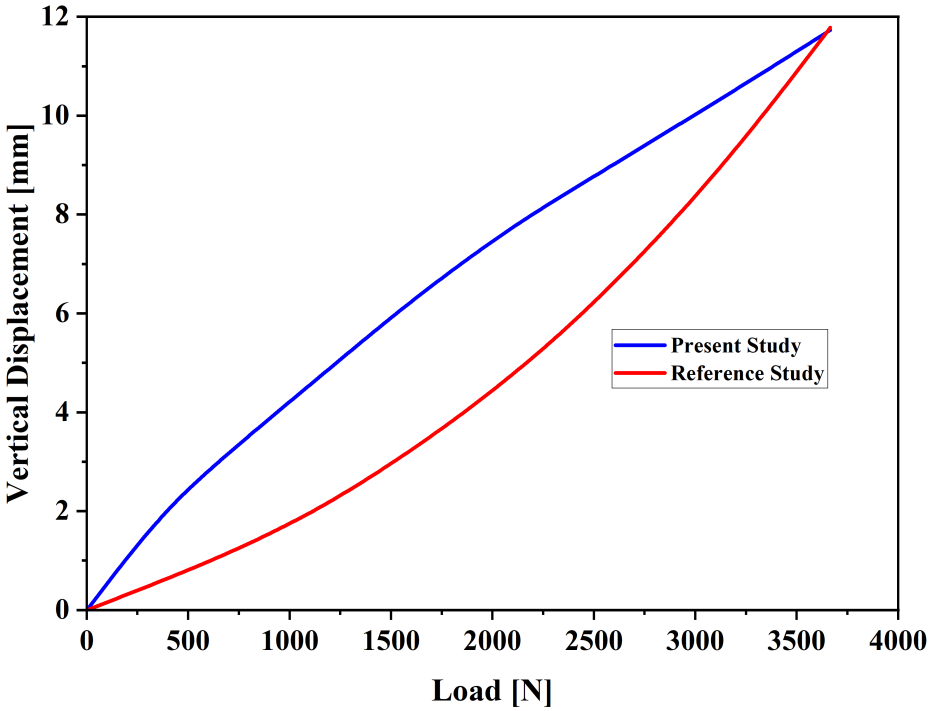

Figure 2.15. The load-displacement response comparison (present study: UPTIS geometry, Tweel material; reference study: Tweel geometry, Tweel material).

3. THE EFFECT OF DESIGN PARAMETERS ON NPT RESPONSE

3.1. Geometric Parameters of the NPT

This section provides a detailed explanation of the geometric parameters that are investigated, as well as the representative quantities used to assess the response of the NPT. The following are the geometric parameters that are examined in the study:

- The thickness of the collapsible spoke
- The angle of the collapsible spoke
- The thickness of the reinforcement ring

The collapsible spoke is located on the structures which connect the reinforcement and the inner ring together. The smallest distance between the two faces of a spoke is defined as the thickness of the collapsible spoke and is shown in Figure 3.1. In this study, the thickness value is restricted from 2 mm to 6 mm due to the design constraint on the geometry of the collapsible spoke of the NPT.

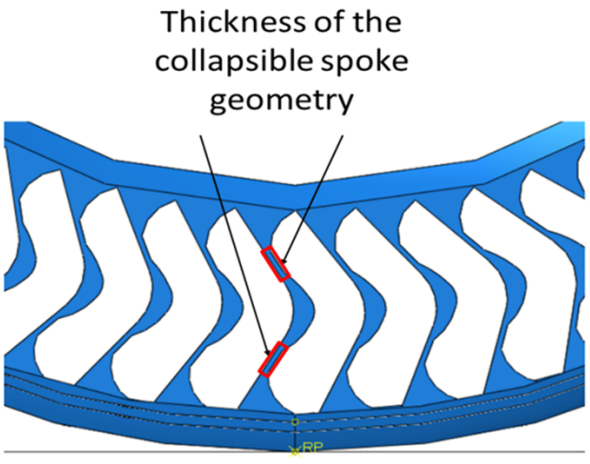

Figure 3.1. The thickness of the collapsible spoke geometry of the NPT.

The angle of the collapsible spoke geometry in the UPTIS-based NPT is measured between the two inner faces of a spoke as shown in Figure 3.2. The original angle of the UPTIS collapsible spoke geometry is 120°. In this study, this value is varied as 122.5°, 125°, 127.5°, and 130°.

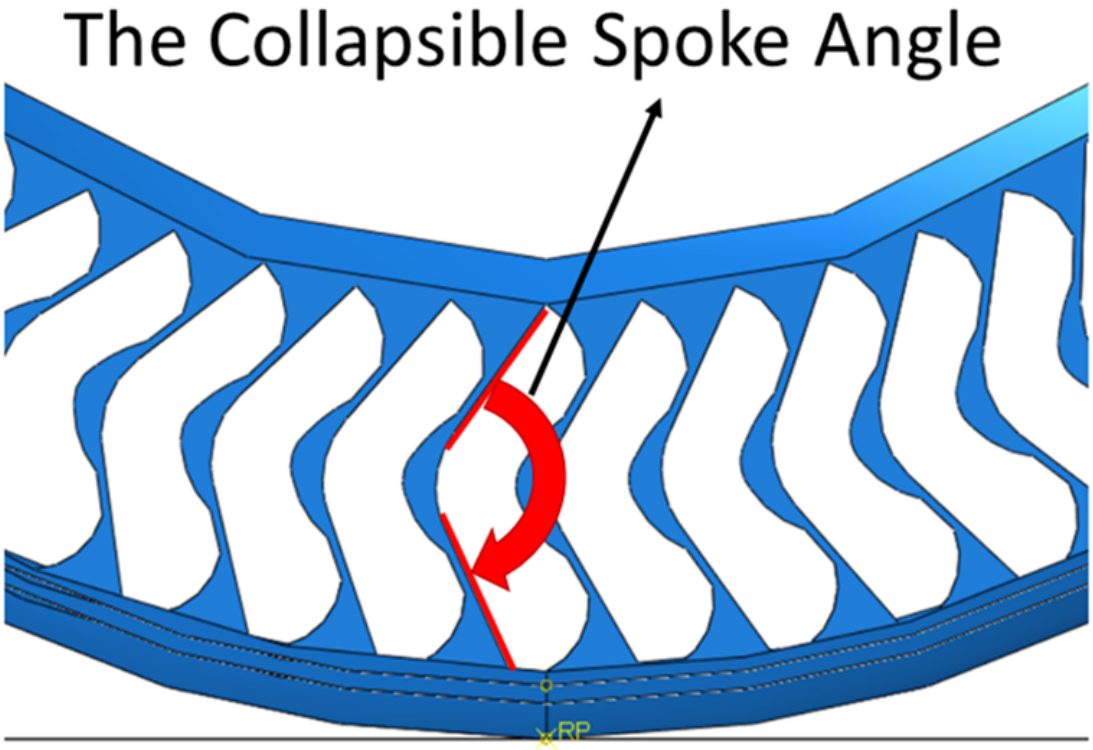

Figure 3.2. The angle of the collapsible spoke of the NPT.

Figure 3.3 shows the thickness of the reinforcement ring of the NPT design. The thickness of the reinforcement ring is altered as 4 mm, 5 mm, and 6 mm in the study. The reinforcement ring ensures that the NPT maintains its shape and can withstand diverse road conditions, ultimately enhancing safety and efficiency during driving.

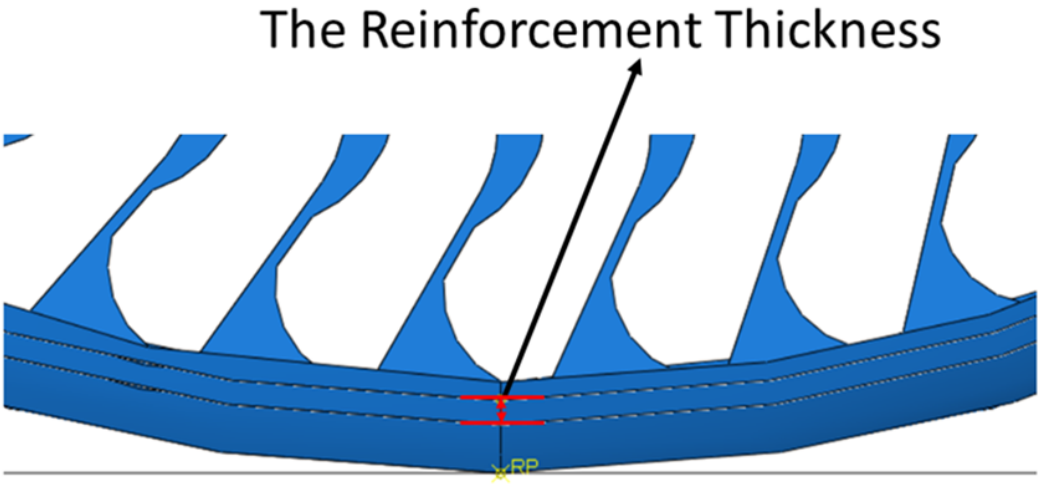

Figure 3.3. The thickness of the reinforcement geometry of the NPT.

In the study, FE simulations for the static footprint loading and rolling are conducted to calculate four different quantities that serve as representative measures of the NPT response. These quantities are chosen to capture key aspects of the NPT's behavior and performance. The four calculated quantities are:

- The vertical displacement
- The vertical stiffness
- The contact pressure
- The rolling resistance

The vertical displacement corresponds to the displacement of the center of the contact surface between the NPT and the road in the loading direction. The vertical stiffness is calculated as the ratio of the applied force and the displacement in the loading direction. The vertical stiffness can be expressed as

$$K = \frac{F}{\delta}, \tag{3.1}$$

where K is the vertical stiffness of the NPT, F represents the applied vertical force, and δ refers to the deformation of the NPT [4].

The contact pressure refers to the distribution of pressure at the interface between

the NPT and the ground surface. It represents the force per unit area exerted by the NPT on the road. This output is taken from ABAQUS directly from the vertical load analysis.

Rolling resistance affects the fuel consumption of vehicles directly, and most tire manufacturers prefer to report the rolling resistance in their product specifications to give an estimated fuel consumption. In this study, the rolling resistance is calculated from the differences in the work done between the beginning and end of the rolling movement of the NPT. In other words, the rolling resistance is described by the amount of energy that is dissipated or lost per unit distance traveled by a rolling tire. The rolling resistance can be formulated as

$$F_R = \frac{W_d}{D}, \tag{3.2}$$

where F_R represents the rolling resistance, W_d is the energy lost or dissipated, and D refers to the distance rolled by the NPT [4].

There are various sources that affect the rolling resistance. As the tire rolls, the components such as the reinforcement ring, the tread, and the spokes undergo deformation. Friction between the NPT and the road is another source of energy loss. The major contribution to the energy dissipation comes from the viscoelastic behavior of the PU, however, this feature was not taken into account in this study.

The vertical load applied to the NPT consists of 3991.306 N, 4903.324 N, and 5638.822 N. For rolling only 3991.306 N vertical load is considered as detailed in Chapter 2.

3.1.1. Thickness of Collapsible Spoke

In the first parametric study, the thickness of the collapsible spoke geometry is altered while the other design parameters of the NPT are kept constant. There are five variants of the NPT including the base model in terms of spoke geometry thickness in this study. These variants have 3 mm, 4 mm, 5 mm, and 6 mm thicknesses of the spoke

geometry in addition to the base model that has a 2 mm spoke thickness. Figures 3.4, 3.5 and 3.6 show the vertical response for 3991.306 N, 4903.324 N, and 5638.822 N, respectively.

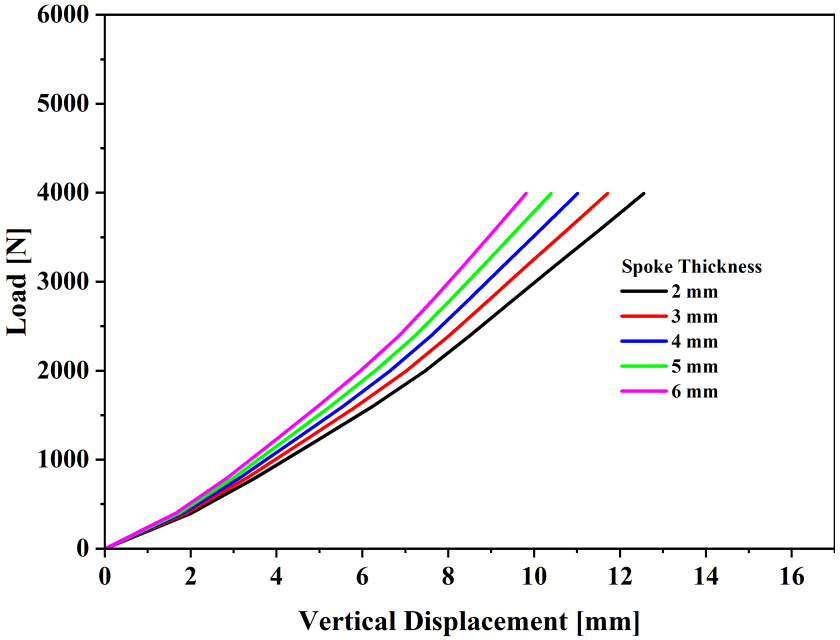

Figure 3.4. The vertical response under 3991.306 N load for various spoke thicknesses.

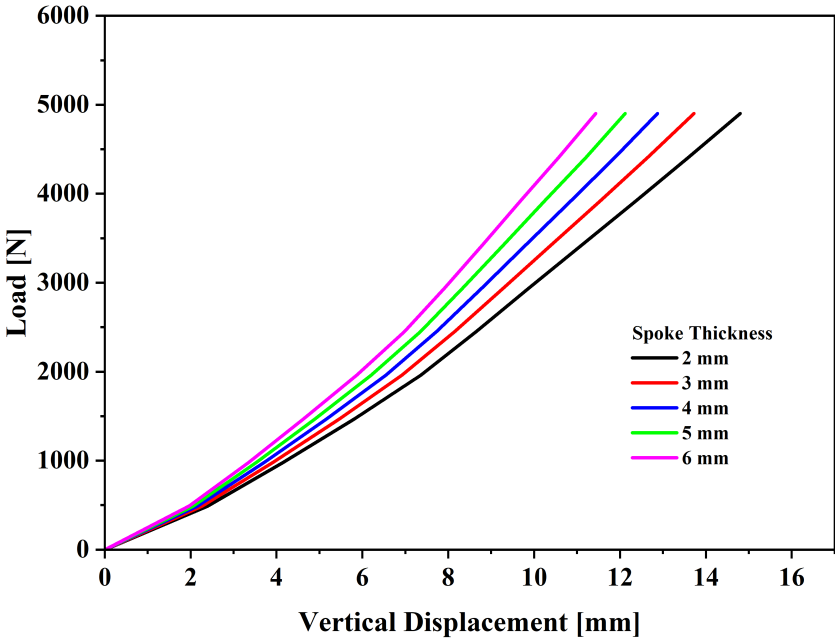

Figure 3.5. The vertical response under 4903.324 N load for various spoke thicknesses.

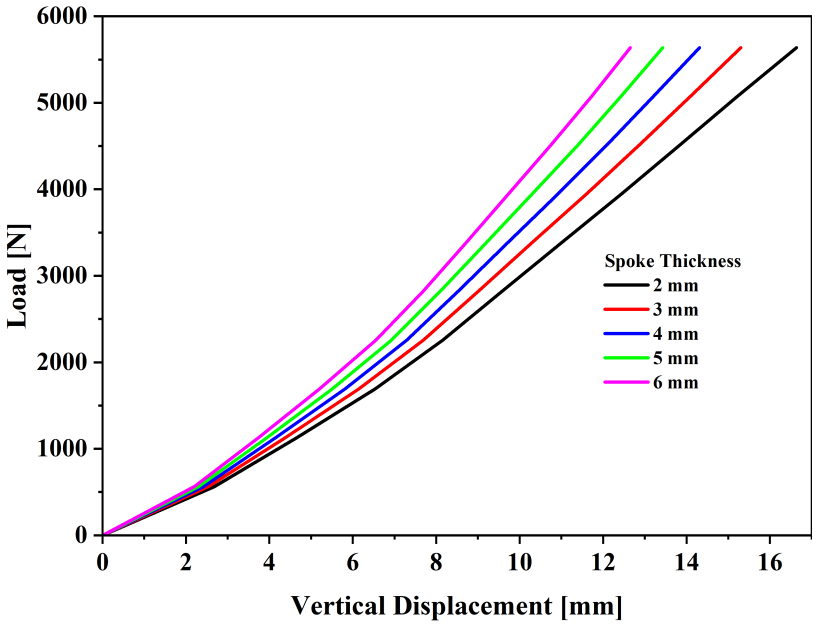

Figure 3.6. The vertical response under 5638.822 N load for various spoke thicknesses.

According to Figures 3.4, 3.5, and 3.6, as expected the vertical deflection of the NPT under the static vertical load is decreased as the spoke thickness is increased. The collapsible spoke geometry connects the tread and the inner ring to each other and as the spoke thickness increases, the structure has more volume. Hence, the NPT has more resistance against the vertical load. The percentile changes in the vertical deflection in terms of thickness and applied loads are summarized in Table 3.1.

Table 3.1. The vertical deflection changes with respect to the base model.

Load [N]	**The vertical deflection decreases as a function of the spoke thickness of NPT [mm]**				
	2 mm	**3 mm**	**4 mm**	**5 mm**	**6 mm**
3991.306	12.5525	6.73%	12.29%	17.23%	21.82%
4903.324 (22.89%)	14.8008	7.26%	13.02%	18.09%	22.72%
5638.822 (41.28%)	16.6329	8.01%	13.97%	19.25%	23.97%

The vertical stiffness of the NPT increases when the thickness of the collapsible spoke geometry is increased as shown in Figure 3.7. Thicker spoke geometry provides more support and resistance against the deformation when the NPT is loaded vertically. The maximum vertical stiffness value is seen for the thickest spoke and the greatest vertical load. The stiffer the NPT, the higher the load-carrying capacity. A stiffer NPT can provide better stability and handling, especially for larger and heavier vehicles.

According to the results of this study when the spoke thickness is increased three-fold, the vertical stiffness increases by about 30%. This can be compared to one study in the literature [15].

Veeramurthy and Ju studied the variation of the vertical stiffness of an NPT type with respect to the change in the spoke thickness at 3000 N vertical load. The results indicated that when the spoke thickness was increased two-fold, the vertical stiffness increased by about 60%. As the geometries and materials of the NPTs are different, the results are expected to be quantitatively different. However, quantitatively the results show the same trend.

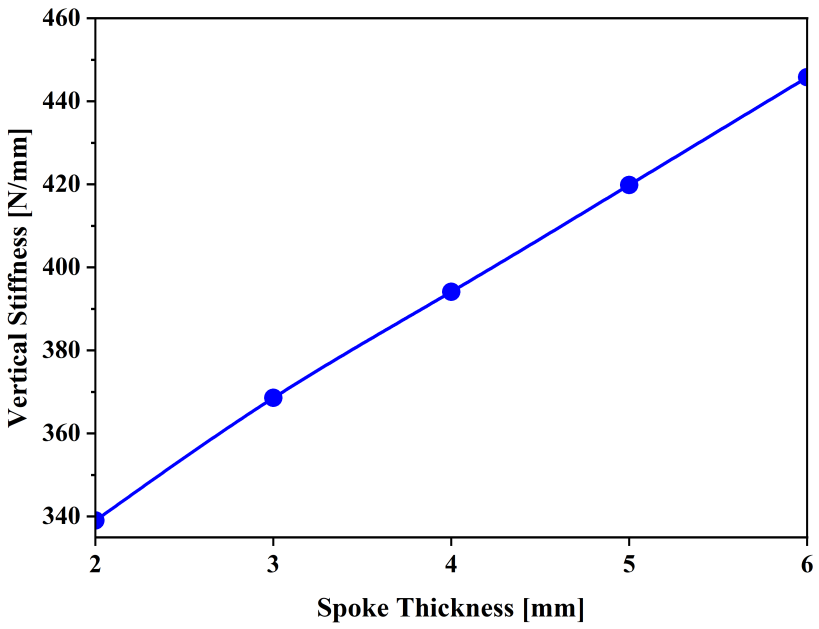

Figure 3.7. Variation of the vertical stiffness of the NPT with the spoke thickness.

The contact path along which the contact pressure is calculated is illustrated in Figure 3.8. The outputs give contact pressure values and their spread on the contact zone during the static footprint loading.

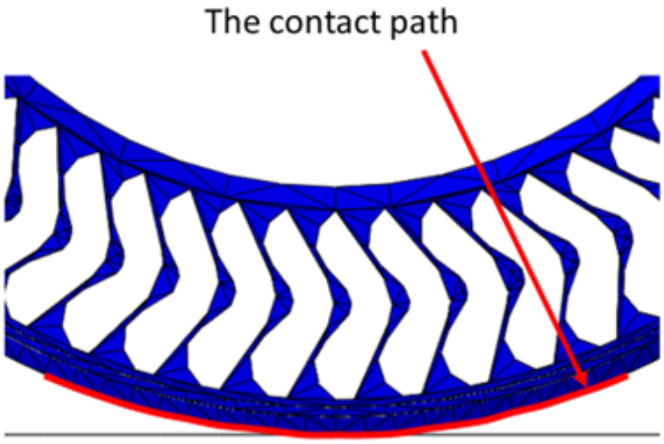

Figure 3.8. The contact path between the NPT and the road.

Figure 3.9, 3.10 and 3.11 show the distribution of the contact pressure for 3991.306 N, 4903.324 N, and 5638.822 N, respectively. In the contact path, the center of the contact point is indicated as zero.

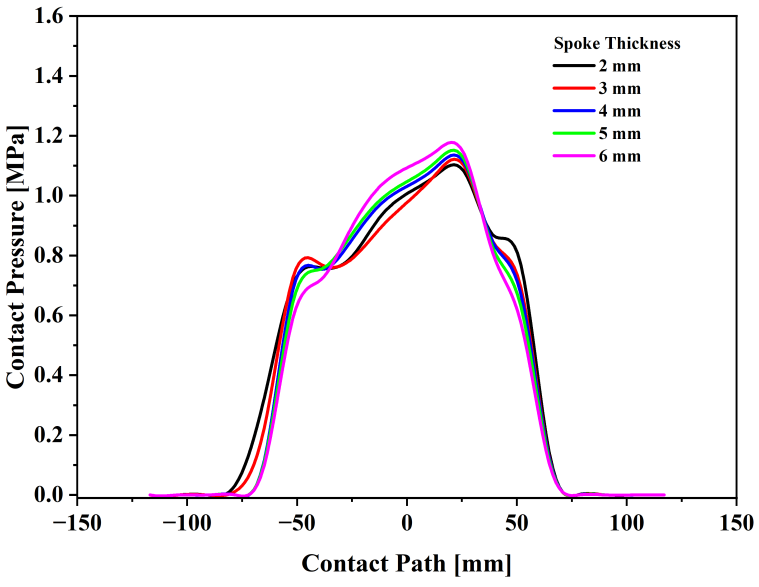

Figure 3.9. Contact pressure under 3991.306 N load and various spoke thicknesses.

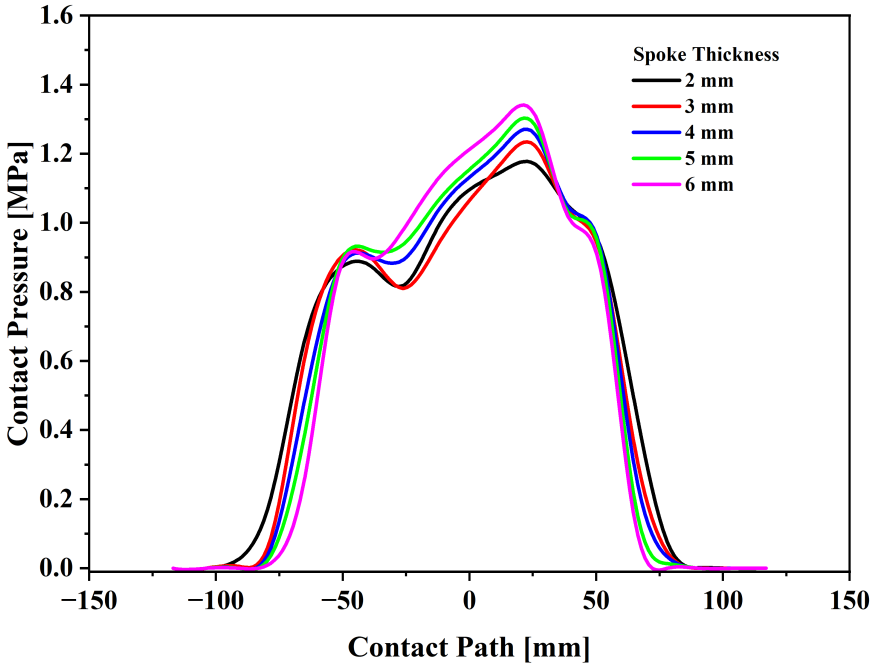

Figure 3.10. Contact pressure under 4903.324 N load and various spoke thicknesses.

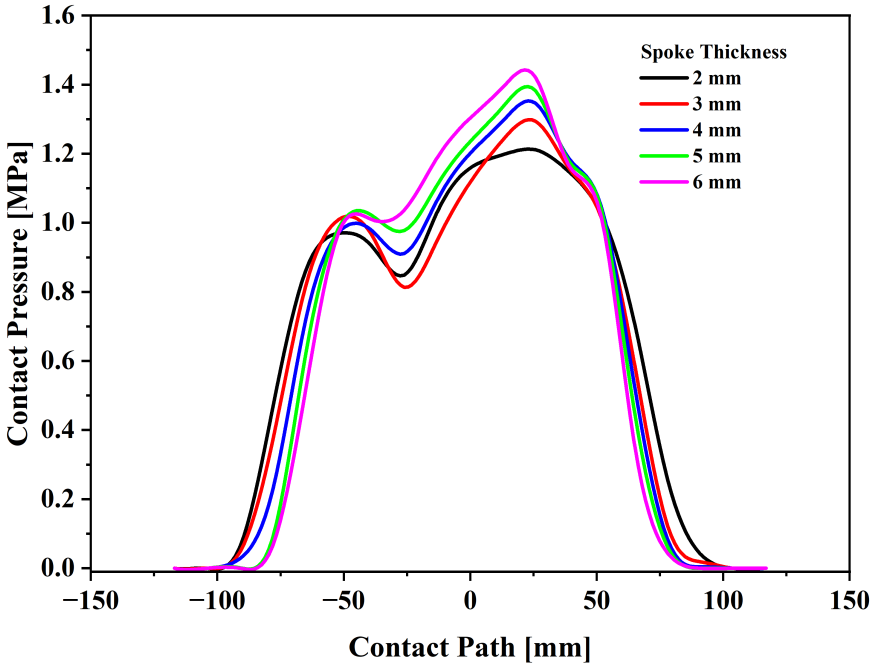

Figure 3.11. Contact pressure under 5638.822 N load and various spoke thicknesses.

According to Figures 3.9, 3.10, and 3.11, when the thickness of collapsible spoke geometry is increased, the maximum contact pressure increases. This is a result of the

NPT being supported by the thicker spokes more effectively. As the NPT has non-symmetric geometrical shapes for the collapsible spoke, the non-symmetric distribution of the contact pressure is observed.

Additionally, the distribution of the maximum contact pressure with respect to the thickness of collapsible spoke geometry is illustrated in Figure 3.12. It is concluded that the maximum contact pressure is observed under the greatest applied load for the largest spoke thickness. Thicker spoke geometry means less deflection of the NPT, hence higher reaction force on the rigid ground against the load applied.

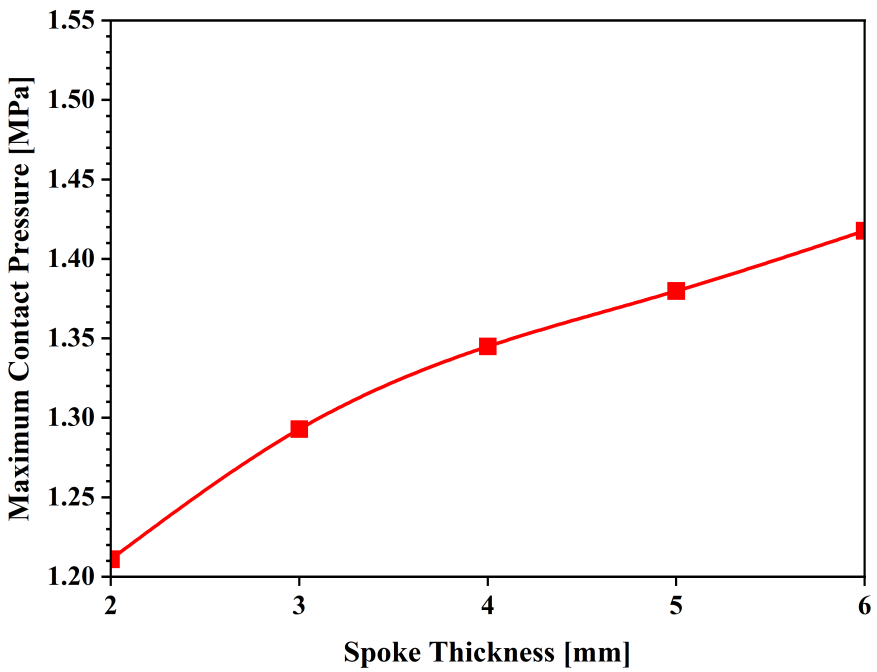

Figure 3.12. Change in maximum contact pressure with spoke thickness under 5638.822 N load.

Figure 3.13 shows the alteration of the rolling resistance with the change in the collapsible spoke thickness of the NPT. Additionally, Table 3.2 shows W_d and D for each spoke thickness value. For W_d, ALLWK, external work, output is used in ABAQUS. Thicker spoke provides more support against the applied loads, resulting in decreased rolling resistance. Thicker spoke behaves more rigidly leading to less energy loss during

rolling. It can be stated that 6 mm thick spoke, the thickest considered in the study, is the most efficient NPT in terms of estimated fuel consumption.

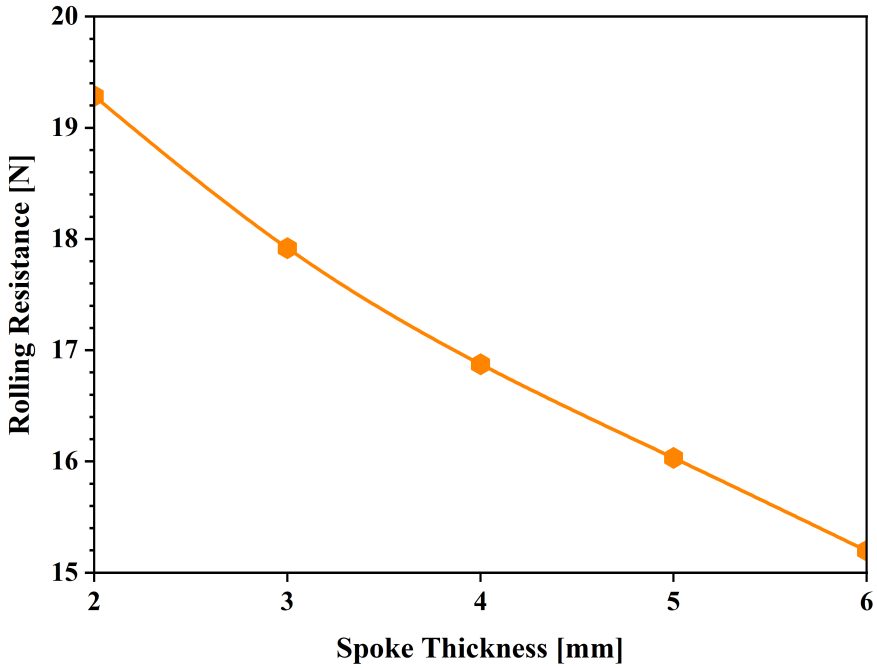

Figure 3.13. Variation of the rolling resistance of the NPT with the spoke thickness.

Table 3.2. W_d, dissipated energy, and D, distance rolled by NPT for various spoke thicknesses.

Parameters	**Spoke Thickness**				
	2 mm	**3 mm**	**4 mm**	**5 mm**	**6 mm**
W_d	19.2855 N.m	17.9183 N.m	16.8746 N.m	16.0306 N.m	15.1965 N.m
D	1 m				

The conclusions regarding the effect of the spoke thickness for static loading are given below:

- Vertical deflection decreases as the spoke thickness increases.
- Contact pressure between the rigid ground and the tread increases as the spoke thickness increases.

- Rolling resistance decreases as the spoke thickness increases.
- Based on the above results it is concluded that to minimize the rolling resistance, therefore, to increase the vehicle range, the spoke thickness should be increased. In this study, the most fuel efficient NPT variant is found to be a 6 mm spoke, which is the highest thickness analyzed.

3.1.2. Angle of Collapsible Spoke

In the second parametric study, the angle of the collapsible spoke geometry of the NPT is changed with other parameters remaining the same.

As in the first parametric study, Section 3.1.1, three different loads, representing the vehicle weight, are applied. During rolling, only the base weight of the vehicle is used for the vertical load. The vertical load-displacement responses for 3991.306 N, 4903.324 N, and 5638.822 N are illustrated in Figures 3.14, 3.15, and 3.16, respectively.

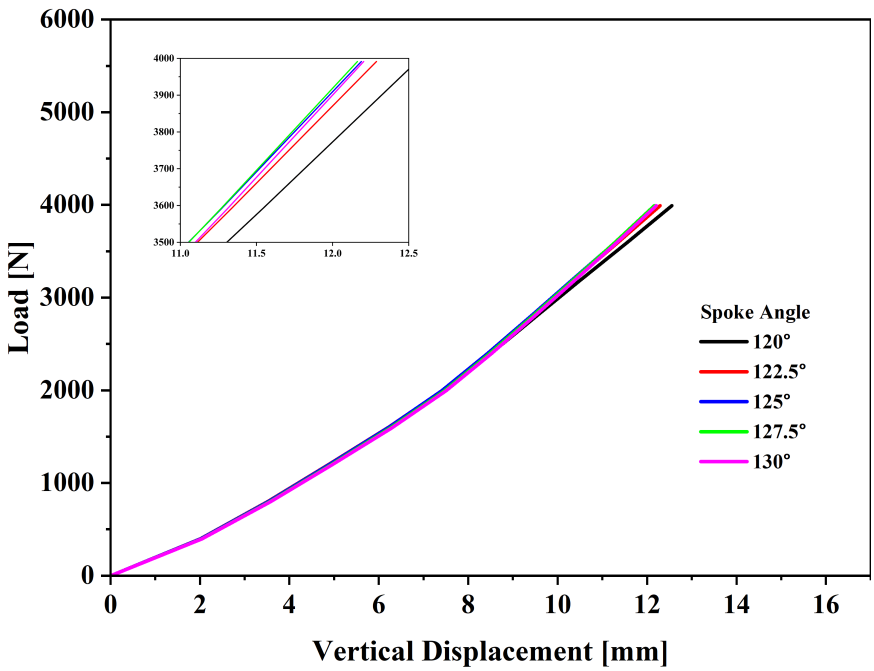

Figure 3.14. The vertical response under 3991.306 N load for various spoke angles.

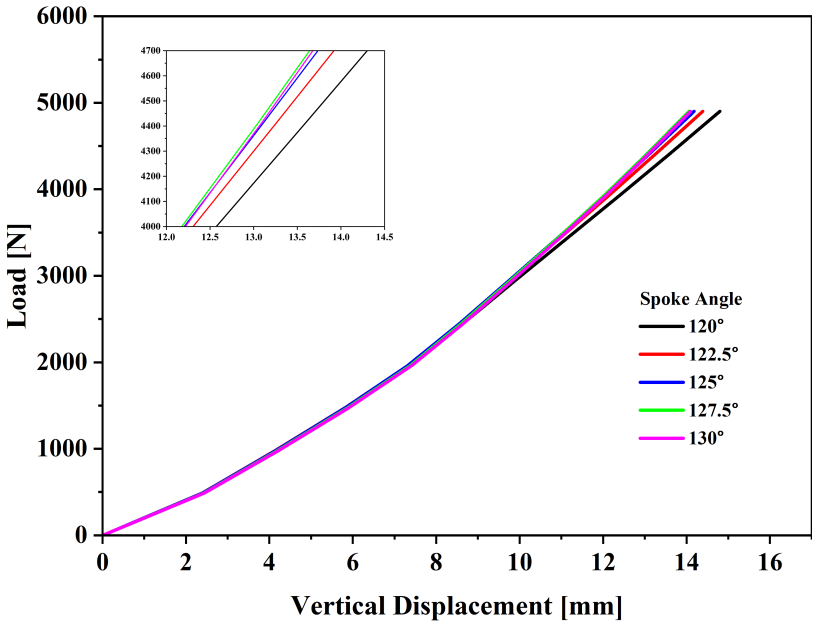

Figure 3.15. The vertical response under 4903.324 N load for various spoke angles.

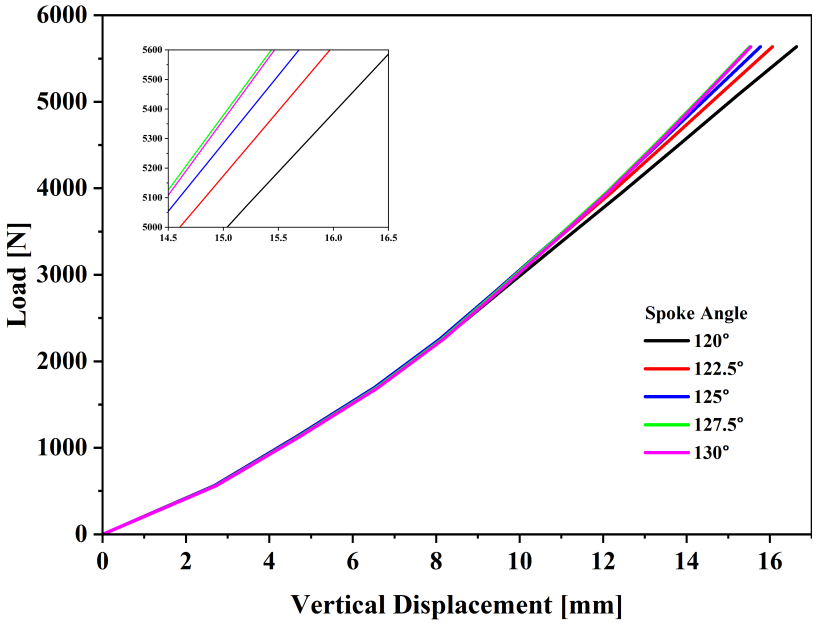

Figure 3.16. The vertical response under 5638.822 N load for various spoke angles.

According to the results initially, increasing the angle of the collapsible spoke geometry reduces the vertical deflection of the NPT. This effect indicates that a higher collapsible spoke angle of the NPT leads to a more rigid structure. However, the

vertical deflection starts increasing again approaching 130°. This is because of the design constraints of the collapsible spoke geometry of the NPT. There is a bump form in the middle portion of the spoke geometry. This unique shape makes the NPT softer at the 130° spoke angle due to the nonsymmetric structure.

The differences can be observed clearly in Table 3.3 which summarizes the vertical deflection values for various loads and spoke angles. At 127.5° spoke angle, the minimum vertical deflection is measured in the static loading. It is therefore concluded that the variant of the NPT which has 127.5° spoke angle offers the most stable driving experience on the roads.

As compared to the spoke thickness effect, for the range considered in the study, the spoke angle effects are much less, 20% for the former compared to 6% for the latter.

Table 3.3. The vertical deflection change according to the base model.

Load [N]	**The vertical deflection decreases as a function of the spoke angle of NPT [mm]**				
	120°	**122.5°**	**125°**	**127.5°**	**130°**
3991.306	12.5525	2.11%	2.90%	3.10%	2.77%
4903.324 (22.89%)	14.8008	2.79%	4.20%	5.01%	4.77%
5638.822 (41.28%)	16.6329	3.46%	5.17%	6.73%	6.56%

The vertical stiffness of the NPT increases when the angle of the collapsible spoke is increased as illustrated in Figure 3.17. The maximum vertical stiffness value is calculated for the 127.5° spoke angle. At 130°, the vertical stiffness is slightly reduced.

The distribution of the contact pressure along the contact path is illustrated in Figures 3.18, 3.19, and 3.20 under 3991.306 N, 4903.324 N, and 5638.822 N loads, respectively. For the lowest applied load as the spoke angle is increased, the contact

pressure increases reaching its maximum value at 125° spoke angle. The contact pressure values at 125° and 127.5° spoke angle are nearly the same. After 127.5°, the contact pressure value begins decreasing. A non-symmetric distribution of contact pressure happens due to the non-symmetric geometrical shapes of the collapsible spoke on the NPT.

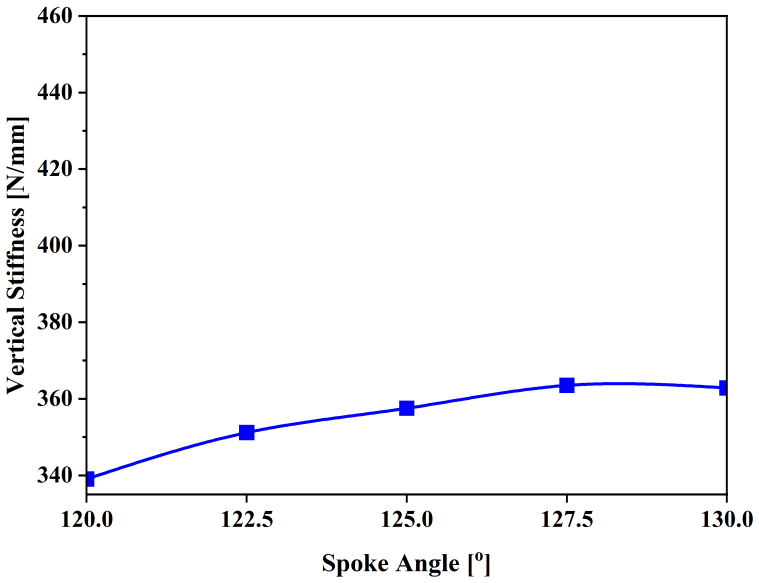

Figure 3.17. The vertical stiffness change with the spoke angle.

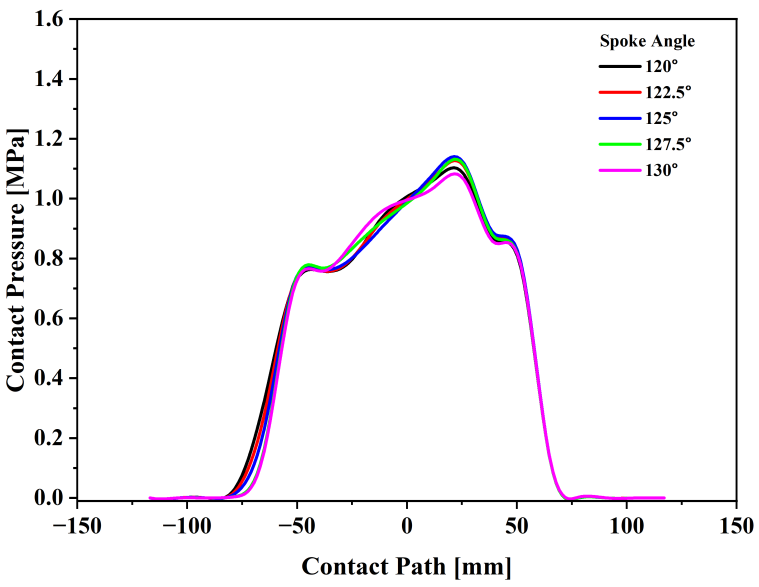

Figure 3.18. Contact pressure under 3991.306 N load for various spoke angles.

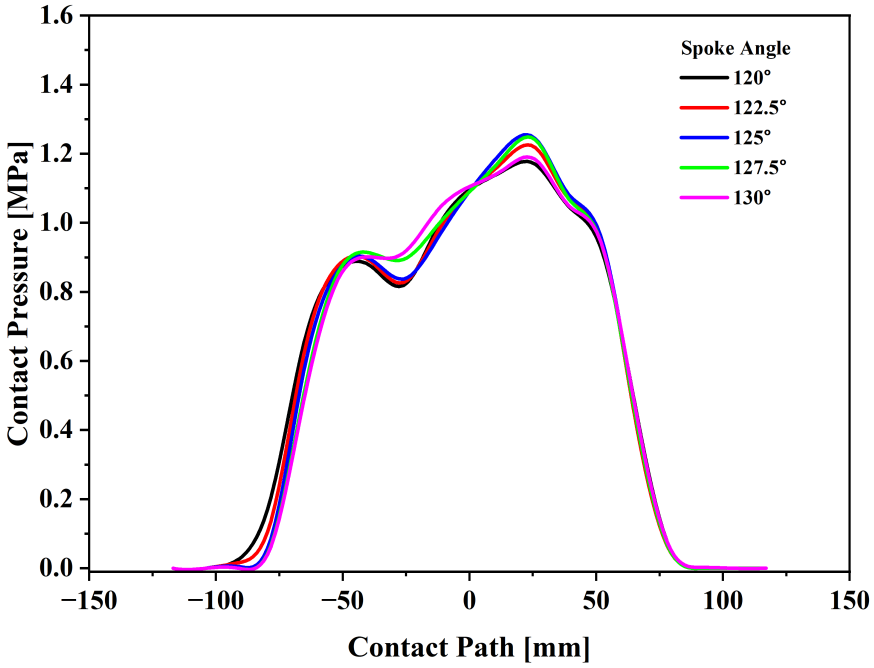

Figure 3.19. Contact pressure under 4903.324 N load for various spoke angles.

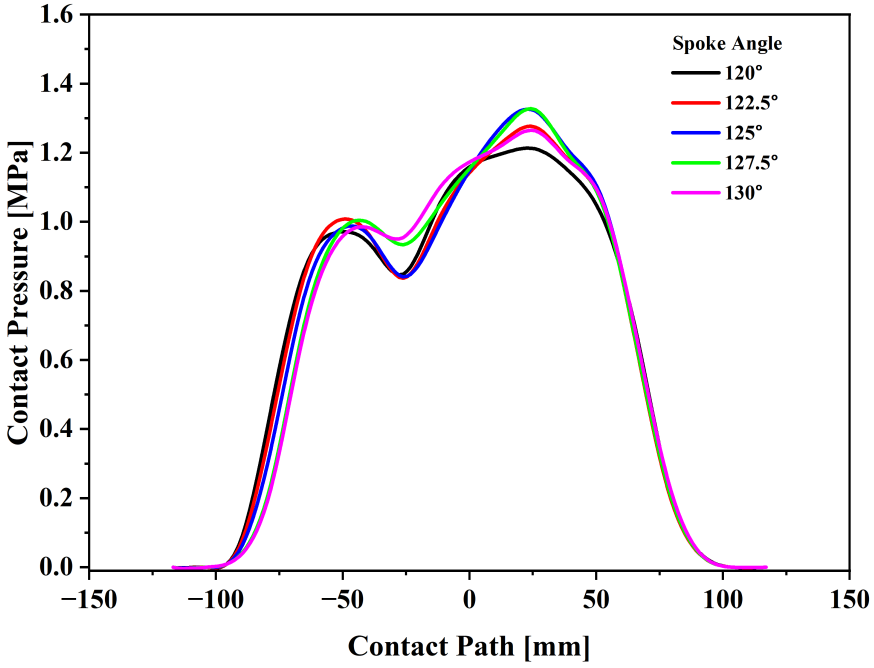

Figure 3.20. Contact pressure under 5638.822 N load for various spoke angles.

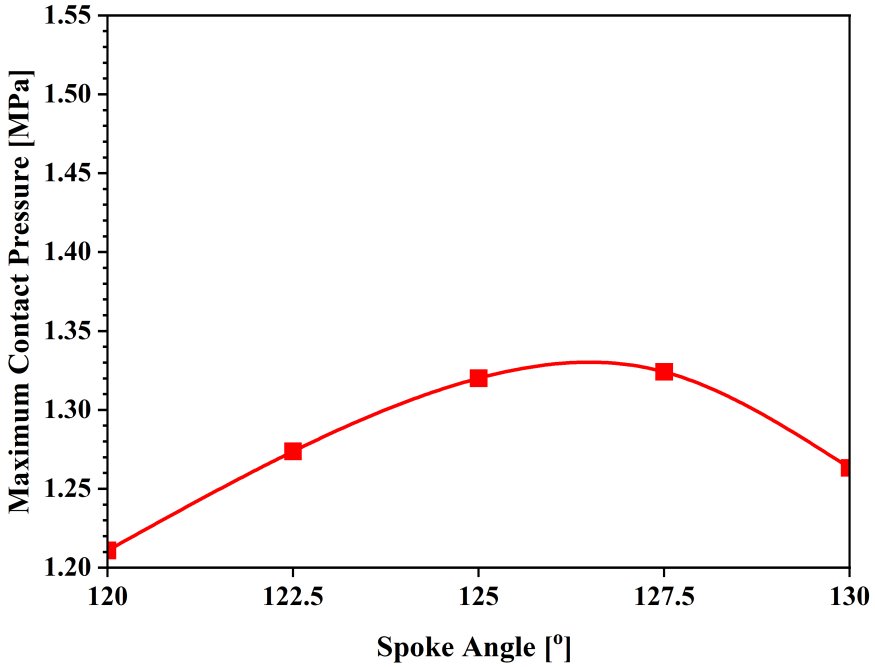

Figure 3.21. Maximum contact pressure change with spoke angle under 5638.822 N load.

Figure 3.21 shows the variation of the maximum contact pressure values with respect to the angle of the collapsible spoke geometry. The maximum contact pressure is calculated for 127.5° spoke angle. The base model of the NPT has the lowest contact pressure.

The rolling resistance with respect to the spoke angles is demonstrated in Figure 3.22. Additionally, Table 3.4 shows W_d and D for each spoke angle value. For W_d , ALLWK output was used in ABAQUS. It is seen that the increase in the spoke angle leads first to decrease, then to increase in the rolling resistance going through minimum at 125° spoke angle. It is therefore concluded that 125° spoke angle variant of the NPT uses the least energy for rolling motion on the road.

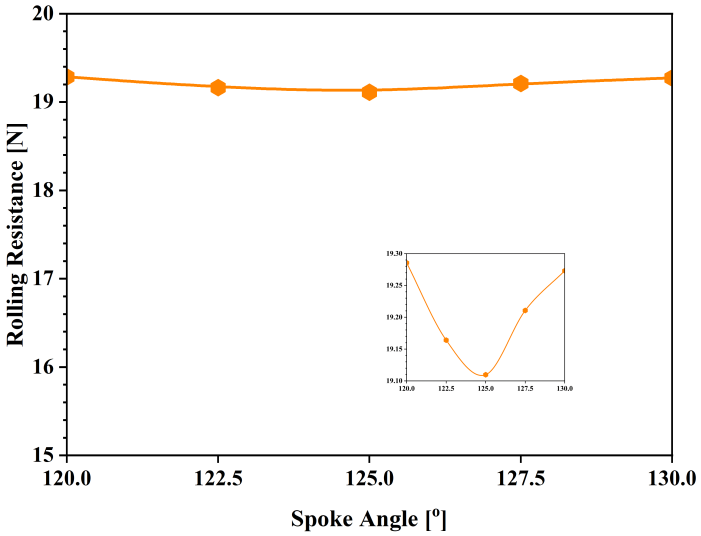

Figure 3.22. Variation of the rolling resistance of the NPT according to spoke angles.

Table 3.4. The distribution of W_d and D according to spoke angles.

Parameters	**Spoke Angles**				
	120°	**122.5°**	**125°**	**127.5°**	**130°**
W_d	19.2855 N.m	19.1640 N.m	19.1096 N.m	19.2106 N.m	19.2730 N.m
D	1 m				

The conclusions regarding the effect of the spoke angle for static loading are given below:

- Changing the spoke angle from 120° to 127.5° leads to a decrease in vertical deflection while increasing it from 127.5° to 130° results in an increase in vertical deflection.
- Changing the spoke angle from 120° to 127.5° leads to an increase in vertical stiffness, with maximum stiffness achieved at 127.5°, while increasing it from 127.5° to 130° results in a decrease in vertical stiffness.
- At spoke angles of 125° and 127.5°, the contact pressure remains almost the same and reaches its maximum. However, there is a significant decrease in contact pressure at a spoke angle of 130°.

- The minimum rolling resistance is found at a spoke angle of 125°. Increasing the angle to 130° leads to an increase in rolling resistance.
- Based on the above results, it is concluded that increasing the spoke angle beyond 125° creates a sharper bump in the middle of the spoke side section, which in turn weakens the NPT by creating stress-raisers.

3.1.3. Thickness of The Reinforcement Ring

In the third parametric study, the thickness of the reinforcement geometry is changed while the other parameters are kept constant. The thickness value is restricted from 4 mm to 6 mm due to the design constraint on the geometry of the NPT. There are three variants of the reinforcement thicknesses including that of the base model. These are 5 mm and 6 mm reinforcement ring thicknesses. The base model has 4 mm reinforcement thickness.

Figures 3.23, 3.24, and 3.25 show the vertical response of the NPT under 3991.306 N, 4903.324 N, and 5638.822 N respectively. The vertical deflection change as a function of the reinforcement ring thickness is summarized in Table 3.5.

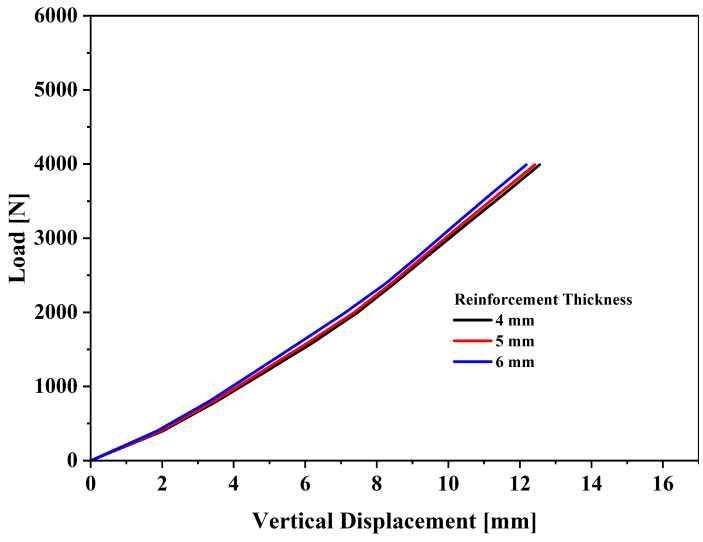

Figure 3.23. The vertical response under 3991.306 N load for various reinforcement ring thicknesses.

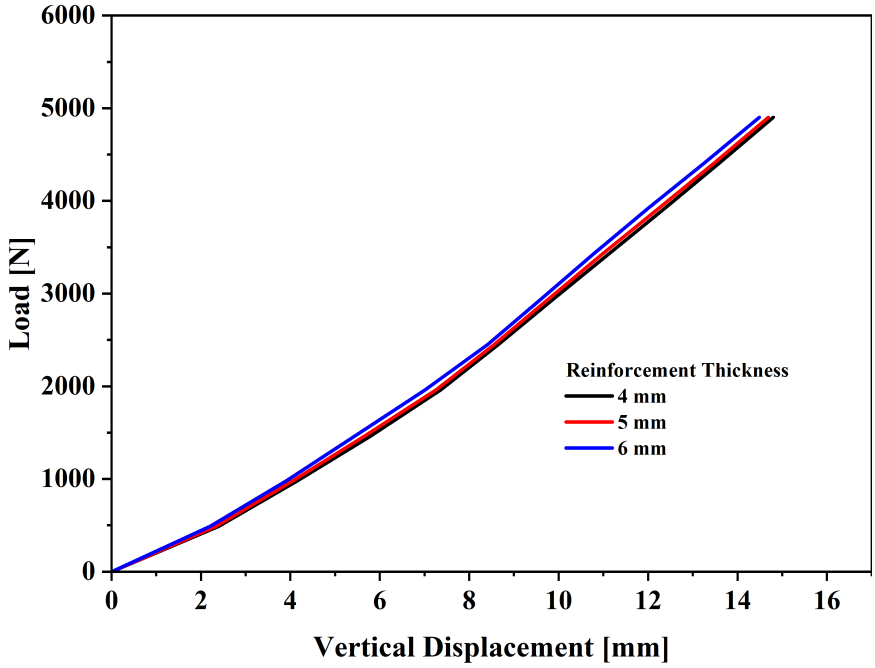

Figure 3.24. The vertical response under 4903.324 N load for various reinforcement ring thicknesses.

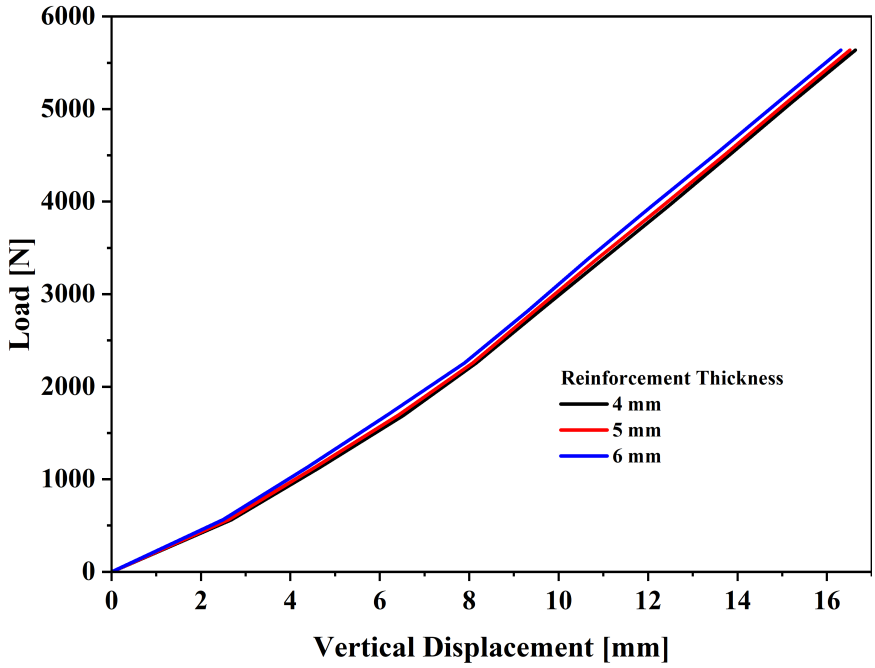

Figure 3.25. The vertical response under 5638.822 N load for various reinforcement ring thicknesses.

Figures 3.23, 3.24, and 3.25 exhibit that there are not significant differences among the vertical response of the variants. Therefore, it is concluded that, for the range considered in the study, the reinforcement thickness does not have any significant effect on the vertical response.

Table 3.5. The vertical deflection change for various loads and reinforcement ring thicknesses.

Load [N]	**The vertical deflection decreases as a function of the reinforcement thickness of the NPT [mm]**		
	4 mm	**5 mm**	**6 mm**
3991.306	12.5525	1.05%	2.95%
4903.324 (22.89%)	14.8008	0.75%	2.11%
5638.822 (41.28%)	16.6329	0.71%	1.94%

As shown in Figure 3.26, the NPT's vertical stiffness increases as the thickness of the reinforcement geometry increases. However, this increase is much smaller than that of spoke parameters.

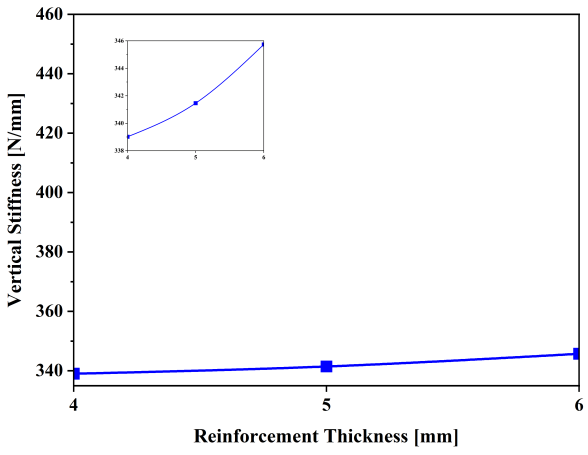

Figure 3.26. Variation of the vertical stiffness of the NPT with the reinforcement thicknesses.

Figures 3.27, 3.28, and 3.29 illustrate the distribution of the contact pressure through the contact path under 3991.306 N, 4903.324 N, and 5638.822 N loads, respectively.

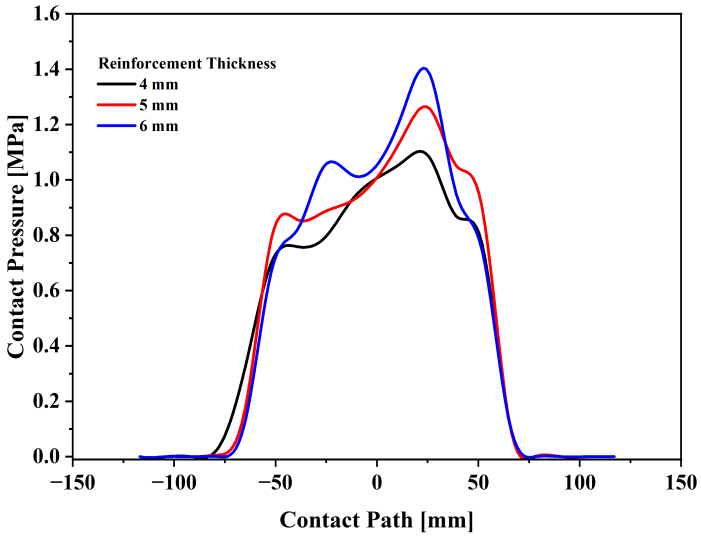

Figure 3.27. Contact pressure under 3991.306 N load and various reinforcement thicknesses.

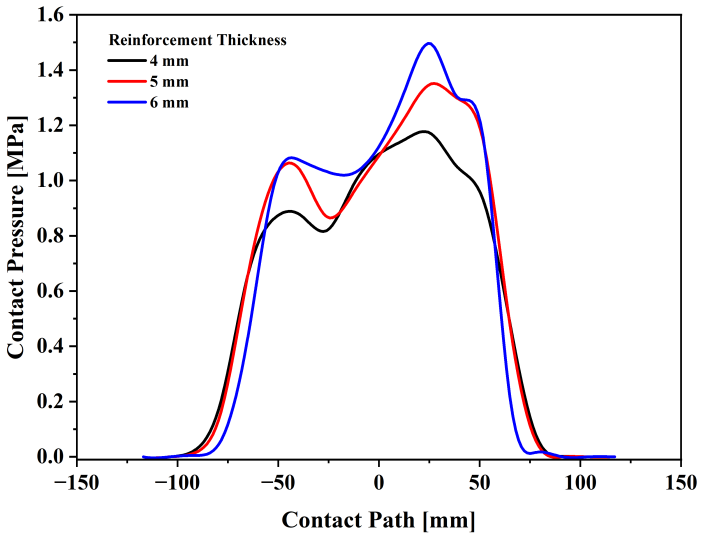

Figure 3.28. Contact pressure under 4903.324 N load and various reinforcement thicknesses.

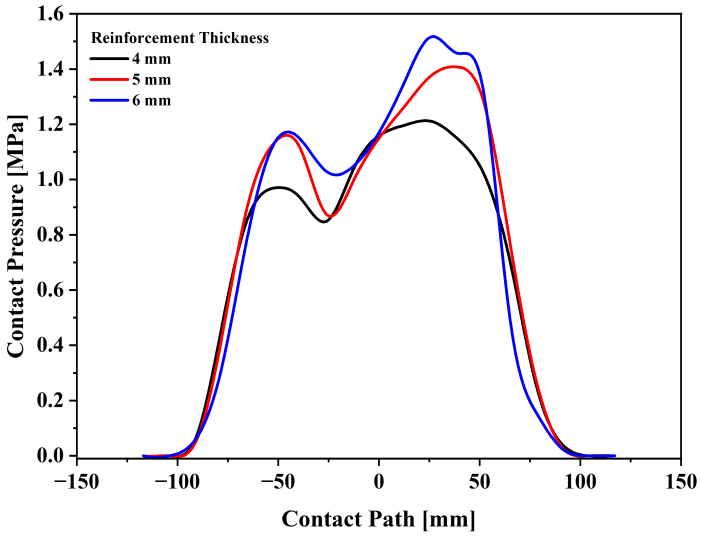

Figure 3.29. Contact pressure under 5638.822 N load and various reinforcement thicknesses.

Figure 3.30 shows the maximum contact pressure in relation to the thickness of the reinforcement ring. It can be seen that the contact pressure increases as the thickness of the reinforcement geometry increases. The maximum contact pressure value is calculated for 6 mm reinforcement thickness, the highest value considered in the study.

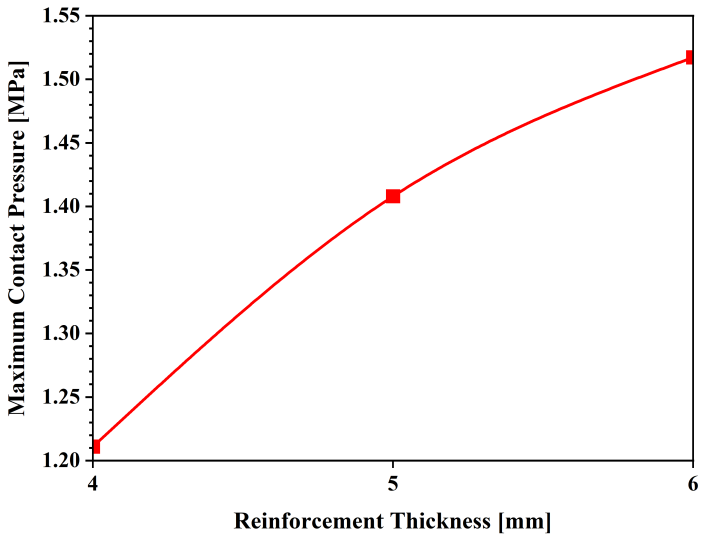

Figure 3.30. The change in maximum contact pressure under 5638.822 N load with respect to the variation in the reinforcement thickness of the NPT.

The rolling resistance of the NPT decreases while the reinforcement ring thickness increases as shown in Figure 3.31. Additionally, Table 3.6 shows W_d and D for each spoke angle value. For W_d, ALLWK output is used in ABAQUS. The base model of the NPT has the maximum rolling resistance value among the variants of the NPT. The least rolling resistance force is observed on the 6 mm reinforcement thickness of the NPT.

The NPT becomes more rigid while the thickness of the reinforcement ring is increased. This means less energy is lost during rolling movement. Furthermore, the more rigid reinforcement ring contributes to carrying more load for the NPT.

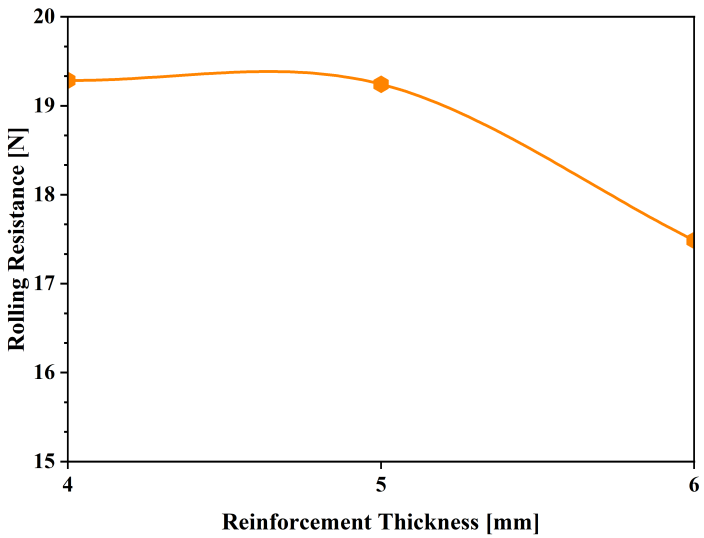

Figure 3.31. Variation of the rolling resistance of the NPT with reinforcement thicknesses.

Table 3.6. The distribution of W_d and D according to the reinforcement thicknesses.

Parameters	**Reinforcement Thicknesses**		
	4 mm	**5 mm**	**6 mm**
W_d	19.2855 N.m	19.2420 N.m	17.4874 N.m
D	1 m		

The conclusions regarding the effect of the reinforcement thickness for static loading are given below:

- Increasing reinforcement thickness has an insignificant effect on the vertical deflection and vertical stiffness.
- Increasing reinforcement thickness leads to a decrease in the rolling resistance.
- Conversely, contact pressure increases with increasing reinforcement thickness.
- According to these results, it can be concluded that the optimal reinforcement thickness for each design output is found to be 6 mm.

Based on the parametric study presented in this chapter, the following conclusions can be made:

Increasing the spoke thickness, vertical deflection can be effectively reduced, while contact pressure between the tire and the road surface is enhanced, contributing to reduced rolling resistance and improved vehicle range. Additionally, the alteration of spoke angles produced distinct effects on vertical deflection, vertical stiffness, and contact pressure. There is an optimum spoke angle for which minimum rolling resistance is obtained. Furthermore, a change in the reinforcement thickness has an insignificant effect on vertical stiffness, while has more pronounced effect on contact pressure and rolling resistance. It is worth to note that upon comparing the effects of the spoke angle with the thickness of the spokes and reinforcement, it was observed that the spoke angle exhibited the least significant design parameter in the vertical displacement, vertical stiffness, contact pressure, and rolling resistance.

4. STEADY-STATE ROLLING ANALYSIS

To assess the dynamic performance of the NPT while rolling, transient analysis must be conducted. Nevertheless, this procedure can be computationally very expensive. An alternative is to perform a steady-state rolling analysis which is computationally quite efficient despite some mesh requirements. In this study, the latter approach is performed using the steady-state transport technique in ABAQUS. In the steady-state rolling analysis the contact patch shape, contact pressure distribution, rolling resistance, and deformed shapes of the NPT are examined. By evaluating these parameters, valuable knowledge can be obtained regarding the tire's dynamic behavior and performance during rolling.

4.1. The Theory of Steady-State Rolling

ABAQUS/Standard offers a specialized analytical technique for simulating the steady rolling behavior of deformable cylindrical bodies on a rigid plane, considering both friction and inertia effects. This method employs a combined Eulerian/Lagrangian approach, where the deformation of the rotating body is described using the Lagrangian method while the rigid body rotation is described using the Eulerian method. By adopting this kinematic approach, the analysis of steady-moving contact is transformed into a simulation that is solely dependent on spatial considerations. This transformation requires continuous lines in the circumferential direction which is realized by generating the 3D FE model from the rotation of the cross-section or from the rotation of a 3D sector [36].

The steady-state rolling principle of a NPT is illustrated in Figure 4.1. At point X_0, the body rotates with a constant angular velocity ω around the symmetry axis T, and at point X_c, it rotates with a constant angular velocity Ω around an axis n.

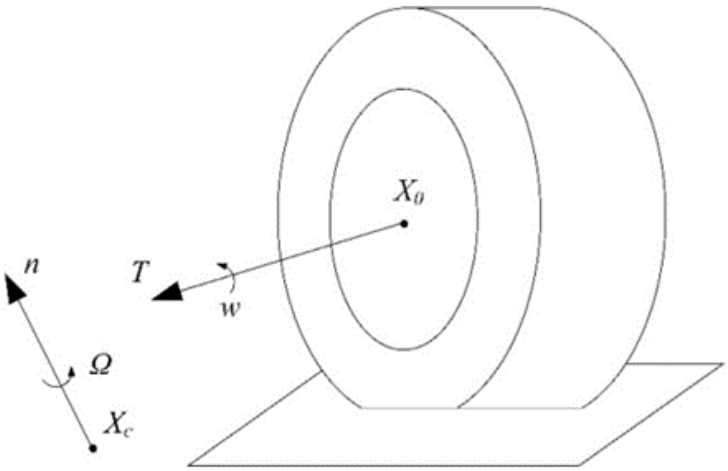

Figure 4.1. Steady-state rolling directions of the NPT.

4.2. Finite Element Model

The FE model of the NPT consists of five main components; inner ring, collapsible spoke, outer ring, reinforcement, and tread as explained in detail in Chapter 2. The material properties for these components are the same as those mentioned in detail in Chapter 2.

The collapsible spoke, inner ring, and outer ring are meshed together to satisfy the continuity requirement in the circumferential direction hence to avoid non-convergence issues during the analysis [36]. For steady-state rolling analysis, choosing the sector with the smallest angle to be as close as possible to the revolution of a two-dimensional cross-section is recommended for NPTs. Figure 4.2 shows the 45° sector FE model used in this study. The final 3D FE mesh of the NPT is composed of 58998 linear tetrahedron elements with hybrid formulation (C3D4H). Interactions and constraints are the same as those in Chapter 2. This means that the friction coefficient between the rigid road and the NPT is equal to 1 during the rolling simulation.

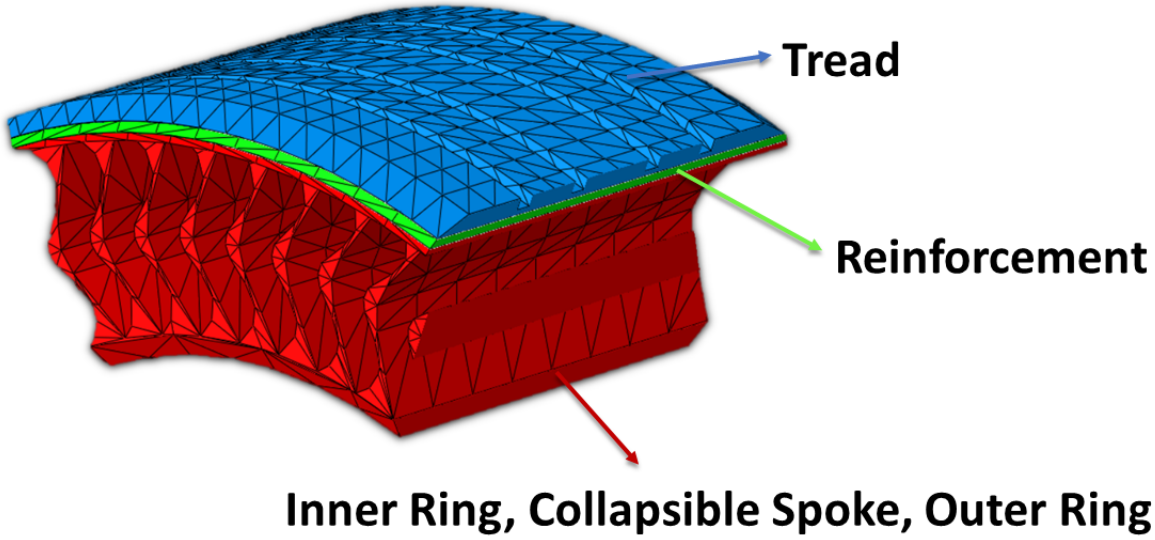

Figure 4.2. 45° sector FE model of the NPT.

4.3. Free-Rolling Condition

The concept of the steady free-rolling state of a tire is fundamental in understanding its behavior during straight-line motion at a constant speed, where both the camber angle and slip angle are assumed to be zero. Camber angle refers to the tilt of a tire relative to the vertical axis when viewed from the front or rear of the vehicle. It is the angle between the tire's vertical axis and the plane of the road surface. Additionally, slip angle is the angular difference between the NPT's actual heading and its desired direction of travel. When a tire experiences lateral forces, such as those during cornering, it can exhibit a slip angle. This state holds significant importance in the fields of vehicle dynamics and tire mechanics, serving as a crucial foundation for investigating dynamic tire performance [37].

When a wheel is in a state of free-rolling, traction, or braking, it will rotate at various angular velocities for the same ground velocity. Typically, the specific combination of angular velocity and ground velocity that leads to free-rolling cannot be predetermined. In order to perform a steady-state transport analysis, where both the angular velocity and the ground velocity need to be determined, the solution for free-rolling

must be obtained indirectly.

During the steady free-rolling process, the NPT's angular velocity is determined by dividing its ground velocity by the effective rolling radius. The effective rolling radius of the NPT should fall in between the loaded radius and the free radius. Therefore, it is possible to estimate the angular velocity of the NPT in a free-rolling state based on the static load simulations.

4.4. Steady-State Analysis

Steady-state rolling analysis occurs in two main steps. In the first step of the analysis, the vertical load is applied at the center of the NPT to perform footprint analysis with zero friction coefficient. Then, the constant ground velocity and variable angular velocity are prescribed at the center of the NPT. The travel direction of the simulation is illustrated in Figure 4.3.

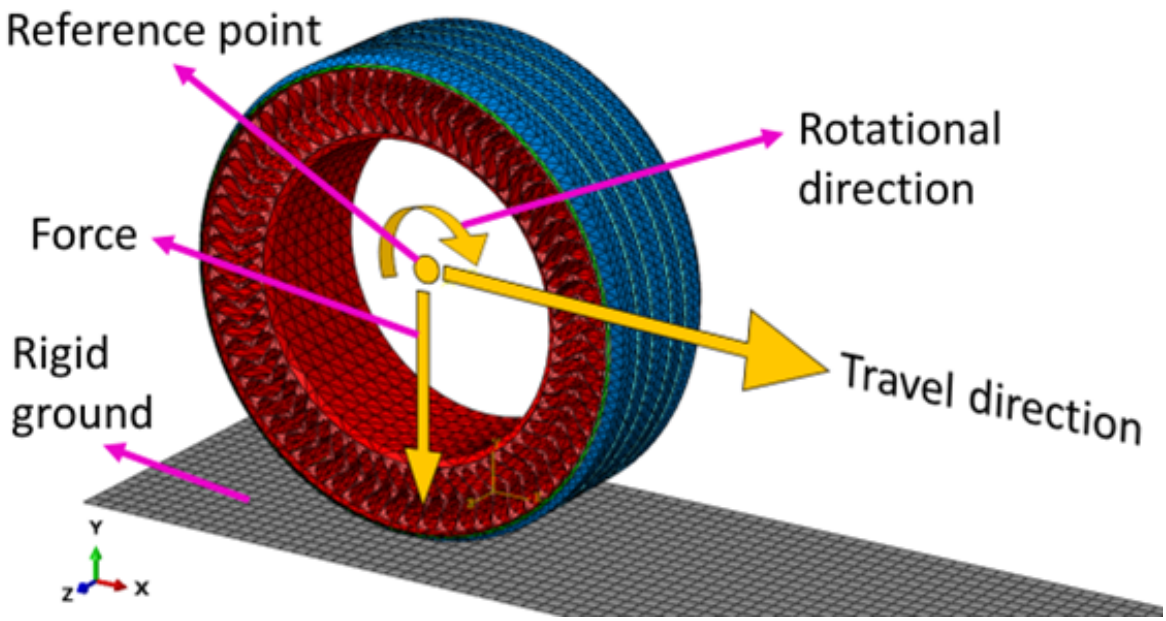

Figure 4.3. 3D FE model of the NPT.

For the footprint analysis, 3991.306 N vertical load is applied at the center of the NPT in the first step of the simulation. In the second step, a constant ground velocity of 60 km/h was assumed for the NPT. The free (undeformed) radius of the NPT is 312.65 mm. According to the vertical deflection result of the static load simulation, the loaded radius of the NPT is 300.10 mm. The effective rolling radius or free-rolling radius is predicted between these two radius values. For the free radius, angular velocity is calculated as 53.24 rad/s, and for the loaded radius is calculated as 55.52 rad/s.

Braking takes place when the NPT's angular velocity decreases to a point where some or all the contact points between the NPT and the road start to slip, causing the NPT's resultant torque to act in the opposite direction compared to the angular velocity of the free-rolling solution. On the other hand, traction occurs during acceleration when the NPT's angular velocity increases sufficiently, causing some or all the contact points between the NPT and the road to slip, and the resultant torque on the NPT acts in the same direction as the angular velocity of the free-rolling solution [38].

In this manner, the angular velocity applied at the center of the inner ring is then varied from 51 rad/s to 57 rad/s so that braking and traction states can be observed during the simulation as shown in Figure 4.4. The state of free-rolling is identified as the angular velocity at which the torque at the center of the NPT is equal to zero by a refined search from 53.9 rad/s to 54.3 rad/s. The NPT is on the free-rolling state at 54.16 rad/s angular velocity for 60 km/h ground velocity as illustrated in Figure 4.5. In the range of 51 rad/s to 54.16 rad/s, the NPT is in a braking state, while between 54.16 rad/s and 57 rad/s, it transits into a traction state based on the angular velocity values.

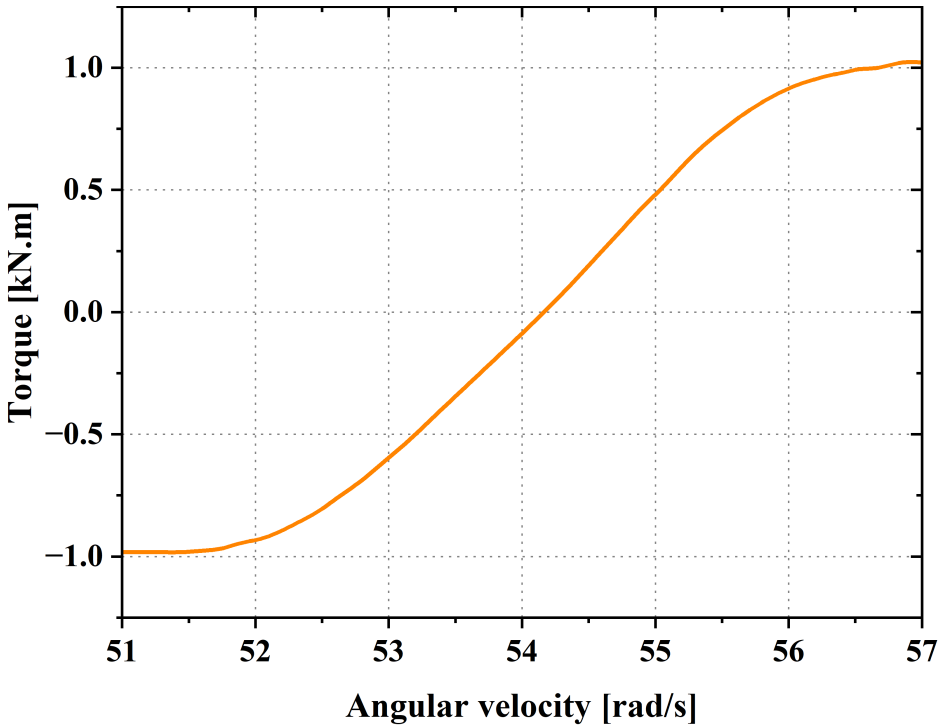

Figure 4.4. Torque distribution along the different angular velocity values.

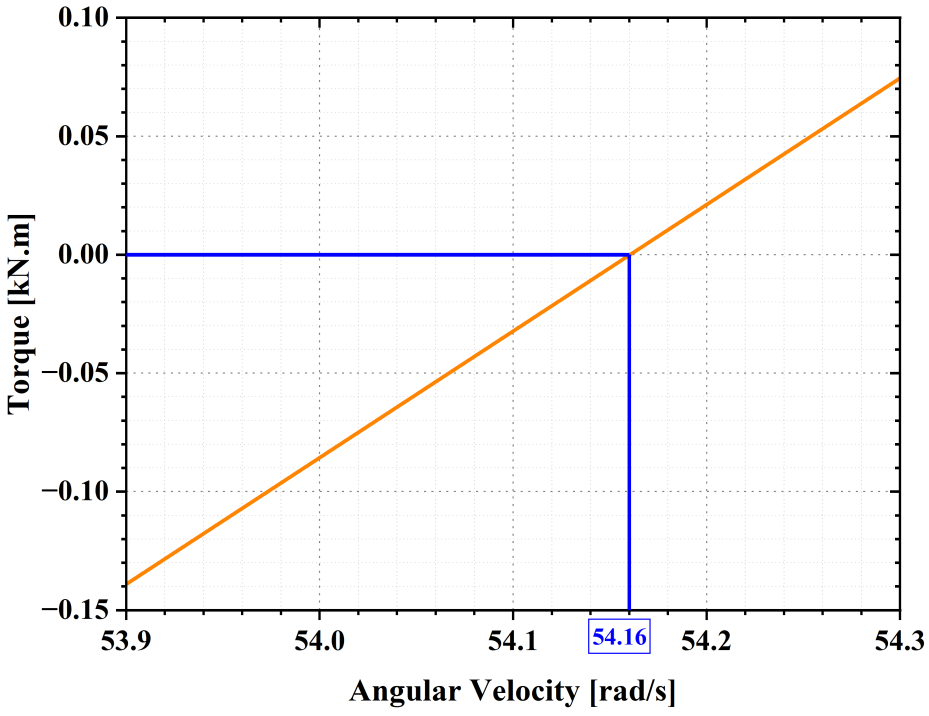

Figure 4.5. Torque distribution for different angular velocity values in refined search.

The effective rolling radius, R_e, is calculated with following equation

$$R_e = \frac{V}{\omega} = \ 307.73 \text{ mm}, \tag{4.1}$$

where V and ω refer to ground velocity and angular velocity, respectively.

Figure 4.6 represents the rolling resistance distribution along with the angular velocity. Unlike the rolling resistance defined as the ratio between the dissipated energy and rolled distance in Chapter 3; in the steady-state rolling analysis, the rolling resistance refers to the force which is parallel to the rigid ground along the traveling direction. It should be noted that the rolling resistance in Chapter 3 refers to a measure for comparison of various design parameters, while in this chapter, it is the actual value used in tire manufacturing. The slip ratio, S [39], is calculated as

$$S = -\frac{(V - \ \omega * R_e)}{V} * 100. \tag{4.2}$$

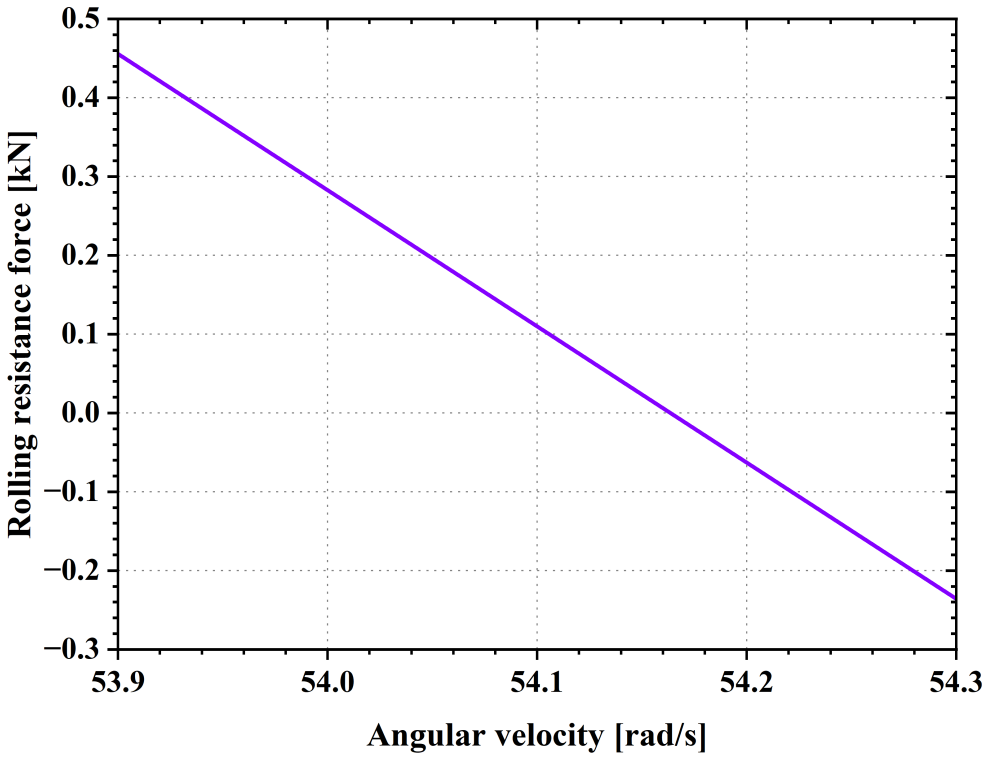

Figure 4.6. Rolling resistance as a function of angular velocity.

Using this information, the longitudinal force versus slip ratio diagram can be created as depicted in Figure 4.7. It is important to note that these diagrams exhibit an asymmetry around the y-axis, indicating distinct behaviors in braking and driving conditions. A linear trend persists for the slip ratio range -1 to 1 as shown in the inset in Figure 4.7. Afterward, the relationship transits into a nonlinear shape, eventually reaching a plateau for higher slip ratio values. This behavior might lead to reduced traction, decreased efficiency, and safety risks because of the unpredictable behavior of handling.

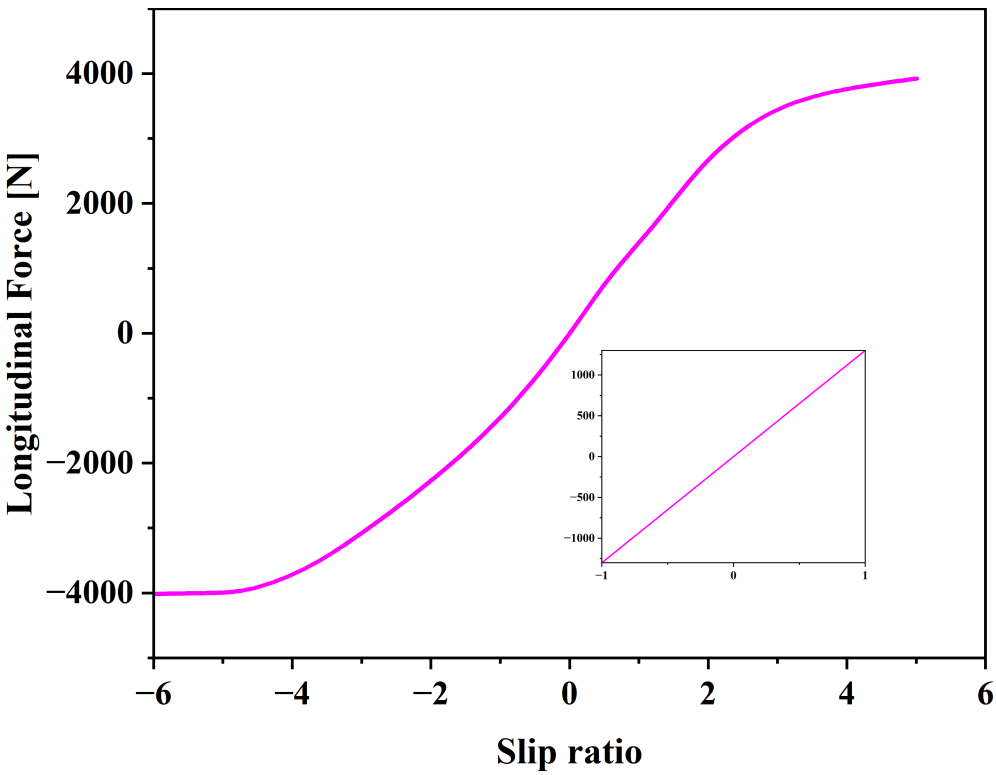

Figure 4.7. Longitudinal force distribution along the slip ratio values.

Additionally, the asymmetrical design of the radial collapsible spoke arms induces varying deformations depending on the negative or positive values of the slip ratio, as illustrated in Figure 4.8. The deformed shapes corresponding to the braking and driving states are overlaid to highlight the alterations. Specifically, during braking, the spokes positioned within the contact patch undergo a leftward translation against the direction of motion. This deformation is a result of the slip velocity, between the tire

and the road. Conversely, in the driving condition, the spokes undergo deformation towards the right, serving as a counterpoint to the braking scenario. The deformation of the spoke while rolling the NPT is obtained at different angular positions as shown in Figure 4.9. Spoke deformation is seen to be bending because of the compression at the lower section of the spoke, which is in contact with the ground. Conversely, the upper part of the spoke is under tension due to supporting the load distributed across the tire. The most significant bending of the spoke occurs at 90°.

Figure 4.8. Comparison of the braking(green) and traction(blue) states of the NPT.

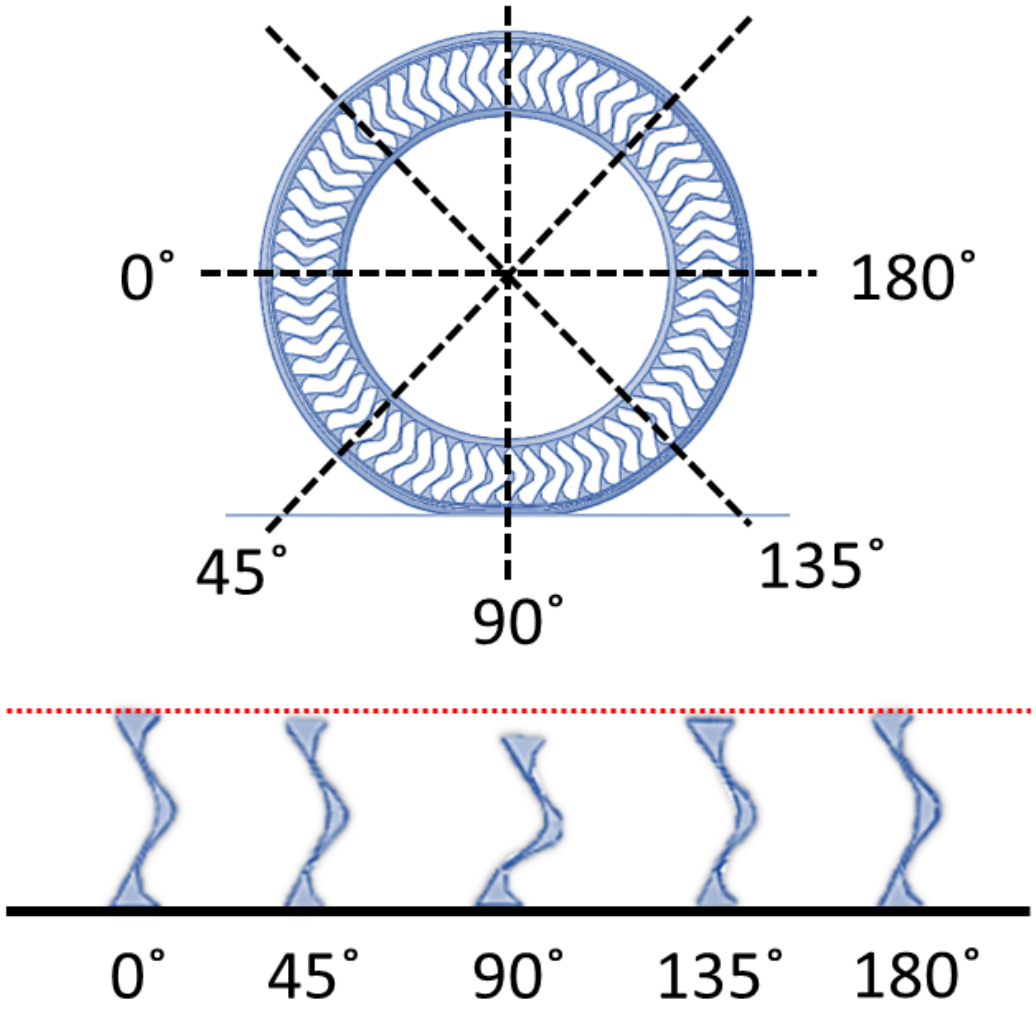

Figure 4.9. The spoke deformation at different angular positions of rolling NPT.

Figure 4.10 presents the contact pressure distribution through the contact region for various states of the NPT during steady-state rolling analysis including Figure 4.10(a) braking state at 51 rad/s, Figure 4.10(b) free-rolling state at 54.16 rad/s, and Figure 4.10(c) traction state at 57 rad/s. In free-rolling state, the side edge of the footprint exhibits a very small high-pressure region. On the contrary, in the braking and traction states of the NPT, the footprint shows disorganized high-pressure distribution through the contact area. This is because of the surface shape of the tread of the NPT. Unlike pneumatic tires, this unique NPT has a flatter tread towards the direction of rotation, not more curved. This can be proved by the rectangular footprint shapes in Figure 4.10. Additionally, the maximum contact pressure value in the free-rolling state

is more than those in the braking and traction state of the NPT because the smallest contact area belongs to the footprint in the free-rolling state.

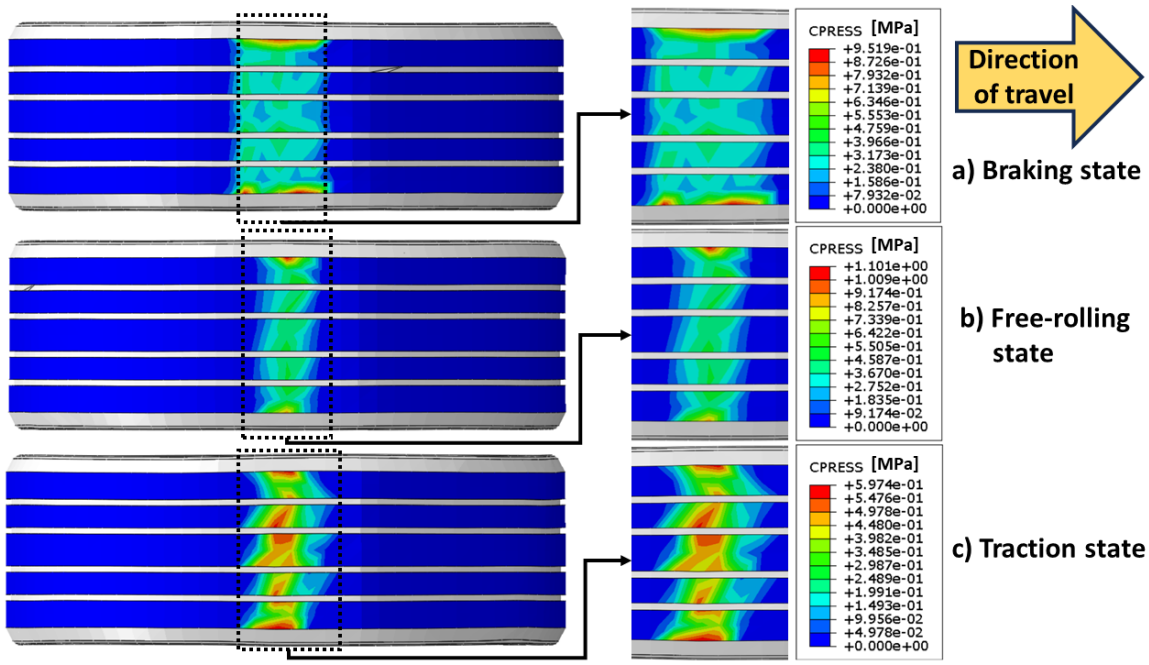

Figure 4.10. Contact pressure distribution of the NPT on (a) braking, (b) free-rolling, and (c) traction states.

This distinction in the contact area and pressure distribution highlights the complex relationship between the rolling state of the NPT and its overall performance. The smallest contact area during free-rolling allows for a more concentrated pressure, increasing the concentration of forces. On the other hand, in the braking and traction states, the pressure is distributed over a larger contact area, resulting in lower maximum contact pressure values. The comparison of the contact pressure distribution in static footprint loading and free-rolling states at the contact area is shown in Figure 4.11. The contact pressure distribution and values are almost the same as expected.

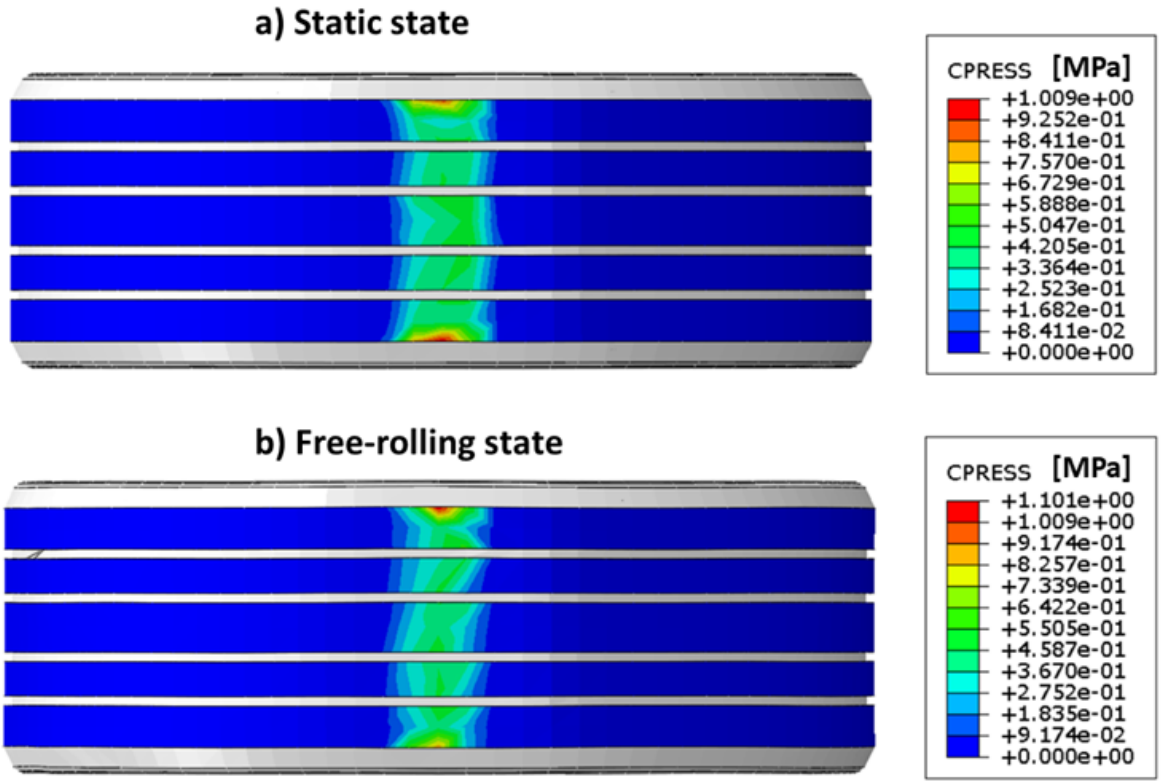

Figure 4.11. Contact pressure distribution of the NPT at the contact area on (a) static and (b) free-rolling state.

The contact pressure results in the braking, free-rolling, and traction states can be compared to one of the studies in the literature [37]. In the reference study, the maximum contact pressure value is located at the center of the contact zone because of the radial tread shape on the tread surface as shown in Figure 4.12. In the present study, the maximum contact pressure value is observed in the middle portion of the contact zone only in the traction state as illustrated in Figure 4.10. In the braking and free-rolling state, the maximum contact pressure value is seen at the side edge of the contact zone as expected due to the flatter tread shape on the tread surface. Moreover, the contact pressure value is almost the same in braking, free-rolling, and traction states in the reference study. However, in the present study, the contact pressure value is different in every state of the NPT. This can be explained by the design and material differences between the NPTs.

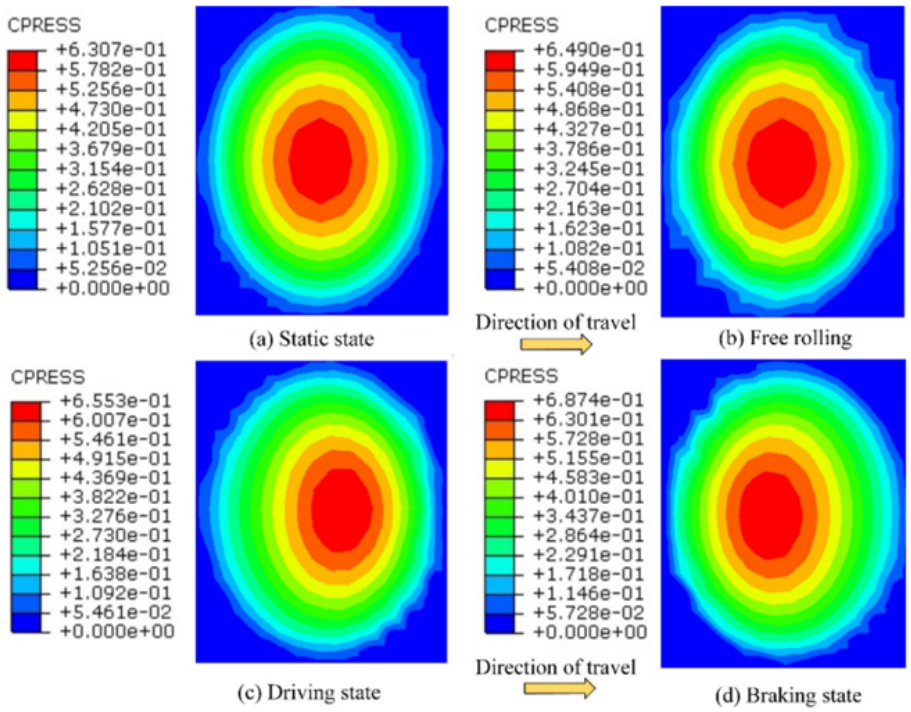

Figure 4.12. Contact pressure distribution of the NPT (in MPa) in the reference study at the contact area on (a) static, (b) free-rolling, (c) driving, and (d) braking states [37]. (Reprinted from Deng et al. 2018. Copyright (2018), with permission from Elsevier.)

Figure 4.13 shows the shear stress distribution at the contact zone on braking, free-rolling, and traction states of the NPT. In the condition of free-rolling, the shear stress value on the tread may be either positive or negative, and overall stress levels are relatively low. In the braking states of the NPT shear stress value is positive. On the contrary, in the traction state of the NPT, the shear stress value is negative. These results agree qualitatively with the study done by Deng et al. [37] and shown in Figure 4.14.

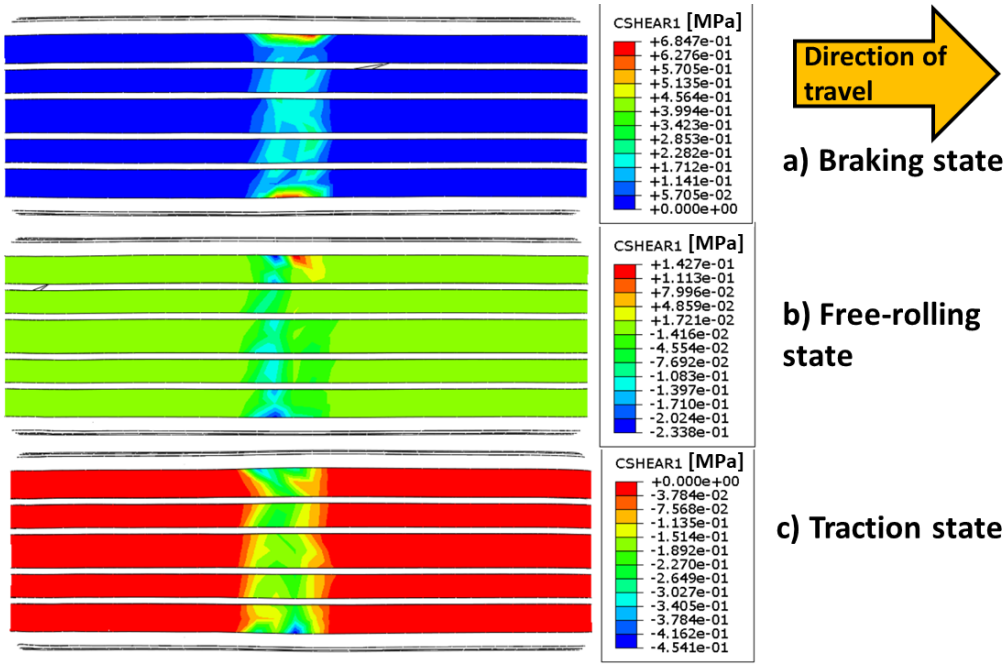

Figure 4.13. Shear stress distribution of the NPT at the contact area on (a) braking, (b) free-rolling, and (c) traction states.

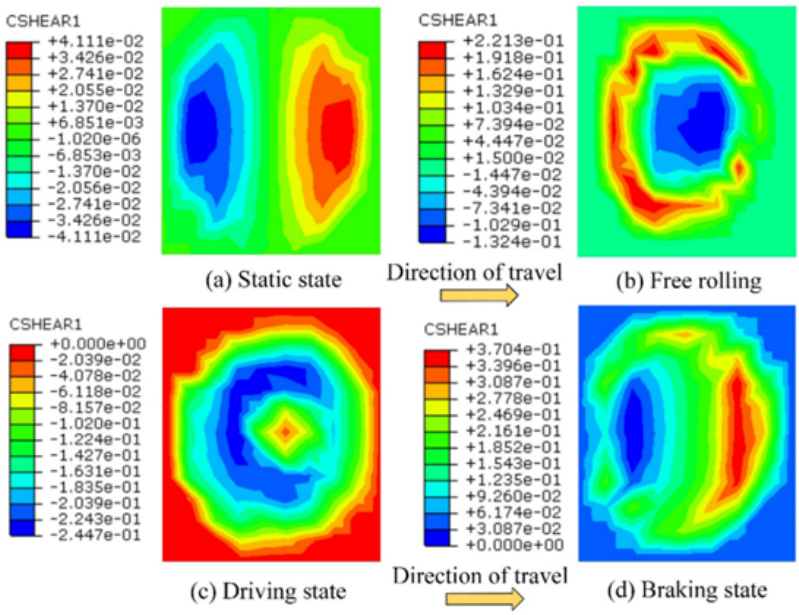

Figure 4.14. Shear stress distribution of the NPT (in MPa) in the reference study at the contact area on (a) static, (b) free-rolling, (c) driving, and (d) braking states [37]. (Reprinted from Deng et al. 2018. Copyright (2018), with permission from Elsevier.)

In conclusion, the highlighted results of the steady-state rolling analysis are given below:

- For the constant ground velocity of 60 km/h, the NPT reaches the free-rolling state at 54.16 rad/s angular velocity.
- The effective radius of the NPT, which is the radius value when the NPT is in free-rolling state, is predicted as 307.73 mm.
- According to the longitudinal force vs slip ratio curve, an asymmetric trend is observed around the y-axis. This shows that the NPT acts differently for braking and tractions states.
- In steady-state rolling for all states, the footprint shape is almost kept as rectangular. This is because of the surface shape. Unlike other tires, this unique NPT has a flatter tread shape towards the direction of rotation, not more curved. This shape might lead to noise and vibration, especially at higher speeds due to inefficient force distribution at the contact area. The design of NPT should be modified to obtain more circular footprint shape.

5. CONCLUSIONS

In this thesis, a parametric study for design optimization of the NPT based Michelin UPTIS model was performed in ABAQUS. In this respect, the effect of spoke thickness, spoke angle, and reinforcement thickness on vertical deflection, vertical stiffness, contact pressure, and rolling resistance was investigated in static footprint and rolling analyses. Desired output is the minimization of the vertical deflection and rolling resistance and the maximization of the vertical stiffness and contact pressure. Additionally, steady-state rolling analysis was performed for the base NPT model to investigate the contact pressure and shear stress distribution in braking, free-rolling, and traction states.

The spoke geometry effect on vertical deflection, vertical stiffness, contact pressure, and rolling resistance was examined while keeping constant the other design parameters. In order to maximize the load-carrying capacity, the vertical deflection should be minimized on the NPT. According to the FEA results, under static loading, the vertical deflection decreases when the spoke thickness increases. Minimizing vertical deflection maximizes vertical stiffness accordingly. It was also observed that as the spoke thickness increases contact pressure increases and rolling resistance decreases. Overall, 6mm spoke, the thickest considered in the study, gives minimum vertical displacement and rolling resistance, and maximum vertical stiffness and contact pressure.

The second NPT design parameter is the angle of the collapsible spoke. Its effect on vertical deflection and stiffness was not as significant as the change due to spoke thickness under all vertical loads. The contact pressure remains the same up to 127.5°, decreasing significantly afterwards. Finally, the rolling resistance is found lowest at 125°, and increasing afterwards. These results have been expected since increasing the spoke angle after 125° sharpens the bump form in the middle of the spoke side section and this makes the NPT weaker.

The third design parameter is the thickness of the reinforcement. As the reinforcement thickness increases, the vertical deflection and rolling resistance decrease, on the other hand, the contact pressure and the vertical stiffness increase. For each design output, the thickest reinforcement gives the greatest structural resistance of the NPT.

In summary, the optimized design would involve a 6 mm spoke thickness, a spoke angle in the range of 120° to 127.5°, and a 6 mm reinforcement thickness. This combined design aims to reduce vertical deflection, enhance contact pressure, minimize rolling resistance, and improve vehicle efficiency. It is worth noting that the best design parameters might be involved in using real-world test data with validation to tune the design further.

The steady-state rolling analysis yielded significant results. Firstly, it was found that at 60 km/h ground velocity, the NPT reaches a free-rolling state at an angular velocity of 54.16 rad/s with the effective radius predicted to be approximately 307.73 mm. Also, the longitudinal force variation with the slip ratio displays an asymmetrical trend around the vertical line where the slip ratio equals zero, implying distinct behavior of the NPT during braking and traction states. NPT's footprint shape remains predominantly rectangular, during braking, traction, and free-rolling states. These findings offer valuable insights into the NPT's performance and characteristics across different rolling scenarios.

In agreement with the results from reference studies in the literature, this study demonstrated a consistent trend in the effects of reinforcement and spoke thickness on the vertical response. Similar to the reference study [4], it was observed that as reinforcement and spoke thicknesses increased, the vertical stiffness and maximum contact pressure were enhanced and rolling resistance was reduced. In addition to that regarding the steady-state rolling analysis, the findings of shear stress in this study match with the reference study [37]. In the braking state, positive stress was observed, on the other hand, in the traction state, negative stress was measured. Furthermore, the rolling resistance values obtained during the transition from braking to traction

states exhibit a similar trend with one of the pneumatic tire example problems in the ABAQUS manual [40]. As expected, the rolling resistance force direction changes from braking to traction states.

5.1. Future Work

The quantitative accuracy of simulations needs a convergence study, which was not carried out in this study. In addition, only linear elements were used in mesh formation. The use of second-order elements may improve the simulation.

In the present study, the effect of geometric design parameters of NPT on its vertical response under static loading was studied. A parallel investigation concerning the material model parameters could be done. This would enable a comprehensive understanding of the behavior of UPTIS under vertical response. Furthermore, the extension of the material model to include viscoelasticity could also be investigated.

Also, the steady-state rolling analysis of the base NPT model may be performed to include the slip angle and camber angle variations. Additionally, at different rolling speeds, the changes in slip ratio could be studied. The suggested optimized design parameters given in this study could also be investigated for steady-state rolling analysis.

REFERENCES

1. Stowe, D., K. Conger, J. D. Summers, P. Joseph, B. Thompson and J. Matthews, "Designing a Lunar Wheel", *International Design Engineering Technical Conferences and Computers and Information in Engineering Conference*, Vol. 43291, pp. 627–639, New York, USA, 2008.

2. Ma, J., J. D. Summers and P. F. Joseph, "Simulation Studies on the Influence of Obstacle on Rolling Lunar Wheel", *International Design Engineering Technical Conferences and Computers and Information in Engineering Conference*, Vol. 44120, pp. 89–100, Montreal, Quebec, Canada, 2010.

3. Ma, J., J. Summers and P. Joseph, "Dynamic Impact Simulation of Interaction between Non-Pneumatic Tire and Sand with Obstacle", *SAE Technical Paper*, 2011.

4. Veeramurthy, M., *Modeling, Finite Element Analysis, and Optimization of Non-Pneumatic Tire (NPT) for the Minimization of Rolling Resistance*, M.S. Thesis, Clemson University, 2011.

5. Ma, J., A. Kolla, J. D. Summers, P. F. Joseph, V. Y. Blouin and S. Biggers, "Numerical Simulation of New Generation Non-Pneumatic Tire (Tweel™) and Sand", *International Design Engineering Technical Conferences and Computers and Information in Engineering Conference*, Vol. 48999, pp. 123–130, San Diego, California, USA, 2009.

6. "Michelin UPTIS", `https://michelinmedia.com/michelin-uptis`, accessed on August 6, 2023.

7. Narasimhan, A., J. Ziegert and L. Thompson, "Effects of Material Properties on Static Load-Deflection and Vibration of a Non-Pneumatic Tire During High-

Speed Rolling", *SAE International Journal of Passenger Cars-Mechanical Systems*, Vol. 4, No. 2011-01-0101, pp. 59–72, 2011.

8. Ju, J., M. Veeramurthy, J. D. Summers and L. Thompson, "Rolling Resistance of a Nonpneumatic Tire Having a Porous Elastomer Composite Shear Band", *Tire Science and Technology*, Vol. 41, No. 3, pp. 154–173, 2013.

9. Petr, M. and O. Novák, "Measurement and Numerical Modeling of Mechanical Properties of Polyurethane Foams", *Aspects of Polyurethanes*, pp. 73–109, 2017.

10. Bates, S. R., I. R. Farrow and R. S. Trask, "3D Printed Polyurethane Honeycombs for Repeated Tailored Energy Absorption", *Materials & Design*, Vol. 112, pp. 172–183, 2016.

11. Hu, S., S. He, Y. Wang, Y. Wu, T. Shou, D. Yin, G. Mu, X. Zhao, Y. Gao, J. Liu *et al.*, "Self-Repairable, Recyclable and Heat-Resistant Polyurethane for High-Performance Automobile Tires", *Nano Energy*, Vol. 95, p. 107012, 2022.

12. Rugsaj, R. and C. Suvanjumrat, "Finite Element Analysis of Hyperelastic Material Model for Non-Pneumatic Tire", *Key Engineering Materials*, Vol. 775, pp. 554–559, 2018.

13. Rugsaj, R. and C. Suvanjumrat, "Dynamic Finite Element Analysis of Rolling Non-Pneumatic Tire", *International Journal of Automotive Technology*, Vol. 22, pp. 1011–1022, 2021.

14. Kim, K., J. Ju and D. M. Kim, "Static Contact Behaviors of a Non-Pneumatic Tire with Hexagonal Lattice Spokes", *SAE International Journal of Passenger Cars-Mechanical Systems*, Vol. 6, No. 2013-01-9117, pp. 1518–1527, 2013.

15. Veeramurthy, M., J. Ju, L. L. Thompson and J. D. Summers, "Optimization of a Non-Pneumatic Tire for Reduced Rolling Resistance", *International Design Engineering Technical Conferences and Computers and Information in Engineering*

Conference, Vol. 54853, pp. 861–868, Washington, DC, USA, 2011.

16. Narasimhan, A., *A Computational Method for Analysis of Material Properties of a Non-Pneumatic Tire and Their Effects on Static Load-Deflection, Vibration, and Energy Loss from Impact Rolling over Obstacles*, M.S. Thesis, Clemson University, 2010.

17. Ju, J., D.-M. Kim and K. Kim, "Flexible Cellular Solid Spokes of a Non-Pneumatic Tire", *Composite Structures*, Vol. 94, No. 8, pp. 2285–2295, 2012.

18. Kucewicz, M., P. Baranowski and J. Małachowski, "Airless Tire Conceptions Modeling and Simulations", *Proceedings of the 13th International Scientific Conference: Computer Aided Engineering 1st*, pp. 293–301, Springer, Wrocław, Poland, 2017.

19. Mathew, N. J., D. K. Sahoo and E. M. Chakravarthy, "Design and Static Analysis of Airless Tire to Reduce Deformation", *IOP Conference Series: Materials Science and Engineering*, Vol. 197, p. 012042, Chennai, India, 2017.

20. Zhang, Z. Z., J. G. Lv, B. Song, S. Y. Guo and F. Gao, "Development of Non-Pneumatic Tire Technology", *Applied Mechanics and Materials*, Vol. 427, pp. 191–194, 2013.

21. Ju, J., B. Ananthasayanam, J. D. Summers and P. Joseph, "Design of Cellular Shear Bands of a Non-Pneumatic Tire-Investigation of Contact Pressure", *SAE International Journal of Passenger Cars-Mechanical Systems*, Vol. 3, No. 2010-01-0768, pp. 598–606, 2010.

22. Zhao, Y., X. Du, F. Lin, Q. Wang and H. Fu, "Static Stiffness Characteristics of a New Non-Pneumatic Tire with Different Hinge Structure and Distribution", *Journal of Mechanical Science and Technology*, Vol. 32, pp. 3057–3064, 2018.

23. Du, X., Y. Zhao, Q. Wang, H. Fu and F. Lin, "Grounding Characteristics of a Non-Pneumatic Mechanical Elastic Tire in a Rolling State with a Camber Angle",

Strojniski Vestnik/Journal of Mechanical Engineering, Vol. 65, No. 5, 2019.

24. Hongxun, F., Z. Youqun, D. Xianbin, W. Qiang and X. Zhen, "Analysis on Influencing Factors of Lateral Stiffness of Mechanical Elastic Wheel", *Journal of Shanghai Jiaotong University*, Vol. 51, No. 7, p. 864, 2017.

25. Hongxun, F., Z. Youqun, L. Fen, D. Xianbin and M. Zhu, "Steady-State Cornering Properties of a Non-Pneumatic Tire with Mechanical Elastic Structure", *Transactions of Nanjing University of Aeronautics & Astronautics*, Vol. 34, No. 5, 2017.

26. Pewekar, M. M. and S. D. Gaikwad, "Strength Validation of Hexagonal Cellular Spoked Non-Pneumatic Tires for Automobiles through Finite Element Analysis", *International Journal of Scientific and Technology Research*, Vol. 4, No. 5, pp. 1044–1055, 2018.

27. Zhao, Y.-q., L.-g. Zang, Y.-q. Chen, B. Li and J. Wang, "Non-Pneumatic Mechanical Elastic Wheel Natural Dynamic Characteristics and Influencing Factors", *Journal of Central South University*, Vol. 22, pp. 1707–1715, 2015.

28. Yang, K. and B. S. El-Haik, *Design for Six Sigma: a Roadmap for Product Development*, McGraw-Hill Education, New York, USA, 2009.

29. Rutherford, W., S. Bezgam, A. Proddaturi, L. Thompson, J. C. Ziegert, T. B. Rhyne and S. M. Cron, "Use of Orthogonal Arrays for Efficient Evaluation of Geometric Designs for Reducing Vibration of a Non-Pneumatic Wheel during High-Speed Rolling", *Tire Science and Technology*, Vol. 38, No. 4, pp. 246–275, 2010.

30. Ramachandran, M., S. Bezgam, L. L. Thompson, J. C. Ziegert, T. B. Rhyne and S. M. Cron, "On the Effects of Edge Scalloping for Collapsible Spokes in a Non-Pneumatic Wheel during High Speed Rolling", *ASME International Mechanical Engineering Congress and Exposition*, Vol. 43864, pp. 685–697, Florida, USA, 2009.

31. "ABAQUS 6.14 Documentation", SIMULIA Corporation, http://130.149.89.49:2080/v6.14/books/usb/default.htm, accessed on August 6, 2023.

32. "Introducing Solidworks, Dassault Systems", Solidworks, 2015, https://my.solidworks.com/solidworks/guide/SOLIDWORKS_Introduction_EN.pdf, accessed on August 6, 2023.

33. "Michelin Tweel", https://michelinmedia.com/tweel/, accessed on August 6, 2023.

34. "Abaqus Analysis User's Manual, Volume 3(v6.8) Materials", Solidworks, 2015, http://130.149.89.49:2080/v6.10/pdf_books/ANALYSIS_3.pdf, accessed on August 6, 2023.

35. "2023 Chevrolet Bolt EV", https://www.chevrolet.com/electric/bolt-ev, accessed on August 6, 2023.

36. "Abaqus Documentation 6.6,", Dassault Systems, SIMULIA Corporation, 2006.

37. Deng, Y., Y. Zhao, F. Lin, Z. Xiao, M. Zhu and H. Li, "Simulation of Steady-State Rolling Non-Pneumatic Mechanical Elastic Wheel using Finite Element Method", *Simulation Modelling Practice and Theory*, Vol. 85, pp. 60–79, 2018.

38. Korunović, N., M. Trajanović, M. Stojković, N. Vitković, M. Trifunović and J. Milovanović, "Detailed vs. Simplified Tread Tire Model for Steady-State Rolling Analysis", *Strojarstvo: Časopis Za Teoriju I Praksu U Strojarstvu*, Vol. 54, No. 2, pp. 153–160, 2012.

39. Genovese, A., D. Garofano, A. Sakhnevych, F. Timpone and F. Farroni, "Static and Dynamic Analysis of Non-Pneumatic Tires based on Experimental and Numerical Methods", *Applied Sciences*, Vol. 11, No. 23, p. 11232, 2021.

40. “Abaqus Documentation 6.6 - 3.1.2 Steady-State Rolling Analysis of a Tire”, Dassault Systems, SIMULIA Corporation, https://classes.engineering.wustl.edu/2009/spring/mase5513/abaqus/docs/v6.6/books/exa/default.htm?startat=ch03s01aex77.html.